

## 11. DETERMINATION OF PRIMITIVE MELT COMPOSITION IN THE NORTH ATLANTIC SEAWARD-DIPPING REFLECTOR SEQUENCES FROM CR-RICH SPINEL COMPOSITIONS<sup>1</sup>

James F. Allan,<sup>2</sup> Lance Forsythe,<sup>3</sup> and James H. Natland<sup>4</sup>

### ABSTRACT

Coring during Ocean Drilling Program and Deep Sea Drilling Project Legs 163, 152, 104, 81, and 38 recovered sequences of altered basalt from North Atlantic seaward-dipping reflector sequences (SDRS) erupted during the initial rifting of Greenland from northern Europe and likely associated with excessive mantle temperatures caused by an impacting mantle plume head. Cr-rich spinel is found abundantly as inclusions and groundmass crystals within the olivine-rich lavas of Hole 917A (Leg 152) cored into the Southeast Greenland SDRS, but only rarely as inclusions within plagioclase in the lavas of the Vøring Plateau SDRS, and it is absent from other cored SDRS lavas from the Rockall Plateau and Southeast Greenland. Eruptive melt compositions determined from inferred, thermodynamically-defined, spinel-melt exchange equilibria indicate that the most primitive melts represented by Hole 917A basalts have  $Mg/(Mg + Fe^{2+})$  at least as high as 0.70 and approach near-primary mantle melt compositions. In contrast, Cr-rich spinels from Hole 338 (Leg 38) lavas on the Vøring Plateau SDRS give evidence for melt with  $Mg/(Mg + Fe^{2+})$  only as high as 0.64. This study underlines that primitive melts similar to those from Hole 917A comprise only a small fraction of the eruptive North Atlantic SDRS melts, and that most SDRS basalts were, in fact, too evolved to have precipitated Cr-rich spinel, with true melt  $Mg/(Mg + Fe^{2+})$  likely below 0.60. The evolved nature of the SDRS basalts implies large amounts of fractionation at the base of the crust or deep within it, consistent with seismic results that indicate an abnormally thick Layer 3 underlying the SDRS.

### INTRODUCTION

An important geological breakthrough of the past decade has been the realization that mantle plumes play an important role in the breakup of continents. Recent models have centered around the role that plume head impingement on continental lithosphere plays in crustal thinning and breakup, accompanied by massive volcanic activity (e.g., White and McKenzie, 1989; Richards et al., 1989; Campbell and Griffiths, 1990). Evidence for this volcanic activity in the early Tertiary North Atlantic volcanic province is supplied both by land exposures and by seaward-dipping reflector sequences (SDRS) that are on the continental shelf and slope. The volcanic nature of the North Atlantic SDRS has been confirmed by drilling (Fig. 1) on Deep Sea Drilling Project (DSDP) Leg 81 (Rockall plateau), DSDP Leg 38 and Ocean Drilling program (ODP) Leg 104 (Vøring Plateau), and ODP Legs 152 and 163 (East Greenland margin). Characterizing the thermal structure of the impinging plumes is critical toward understanding their effects, with estimates of the plume core "excess" temperatures (as compared to the surrounding ambient mantle temperatures) varying widely (100°–300° above the surrounding ambient mantle; see Schilling, 1991; Ribe et al., 1995; and White et al., 1995). In addition, an understanding of the thermal environment of melting is necessary to define the nature of the plume head as it impinges on the continental lithosphere. Fundamentally, does voluminous basaltic volcanism result from an abnormally hot mantle, from large amounts of decompression melting associated with lithospheric thinning, or both? Integration of the drilling results

with other onland studies indicates that decompression melting of a rapidly emplaced, hot plume head was the most likely source for the North Atlantic SDRS (Larsen and Saunders, 1998).

Samples from Legs 163 (Duncan, Larsen, Allan, et al., 1996) and 152 (Larsen, Saunders, Clift, et al., 1994; Larsen and Saunders, 1998) define a nearly complete stratigraphic record of the volcanic evolution of the East Greenland SDRS along a transect at 63°N, with inception of subaerial basaltic volcanism dated at 61–62 Ma (Sinton and Duncan, 1998). These samples are valuable for studying melt generation, transport, and storage processes during continental breakup. In addition, samples from Site 988 (at 66°N on the East Greenland margin), together with samples from Legs 104 (Eldholm, Thiede, Taylor, et al., 1987), 81 (Roberts, Schnitker, et al., 1984), and 38 (Talwani, Udintsev, et al., 1976) allow an examination of geochemical gradients away from the proposed sites of plume impingement.

A key geochemical parameter for characterizing the crustal and mantle thermal regime during continental breakup is the determination of melt Mg# ( $Mg/[Mg + Fe^{2+}]$ ) in the rift magmatic system ( $Fe^{2+}$  is assumed throughout this paper to represent 90% of total Fe, crudely approximating the quartz-fayalite-magnetite oxygen buffer). Melt Mg# reflects a combination of the extent of partial melting (mantle temperature) (Takahashi and Kushiro, 1983; Klein and Langmuir, 1987; Kinzler and Grove, 1992; Niu and Batiza, 1991) and crystal fractionation (effects of cooling, primarily in the lithosphere or at its base; Basaltic Volcanism Study Group, 1981). Picrites were recovered during Leg 152, leading to possibilities that near-primary melts were sampled (Larsen, Saunders, Clift, et al., 1994; Larsen et al., 1998). These highly magnesian lavas may have originated from either abnormally hot mantle or from high amounts of shallow mantle melting during continental breakup (McKenzie and Bickle, 1988; Larsen et al., 1998). Determination of true magmatic melt Mg# compositions for these and other SDRS lavas, therefore, would place direct constraints on plume head thermal influence and the resulting shallow magmatic thermal regime during initial rifting, subsequent continental breakup, and early seafloor spreading.

A significant problem in the interpretation of whole-rock, major element data from all recovered SDRS samples results from their al-

<sup>1</sup>Larsen, H.C., Duncan, R.A., Allan, J.F., Brooks, K. (Eds.), 1999. *Proc. ODP, Sci. Results*, 163; College Station, TX (Ocean Drilling Program).

<sup>2</sup>Department of Geology and Geophysics, Texas A&M University, College Station, TX 77845, U.S.A. (Present address: Ocean Drilling Program, National Science Foundation, 4201 Wilson Blvd., Arlington, VA 22230, U.S.A.) jallan@nsf.gov

<sup>3</sup>Departamento de Geología, CICESE, Ensenada, BJ, Mexico.

<sup>4</sup>Division of Marine Geology and Geophysics, Rosenstiel School of Marine Sciences, University of Miami, Coral Gables, FL 33124, U.S.A.

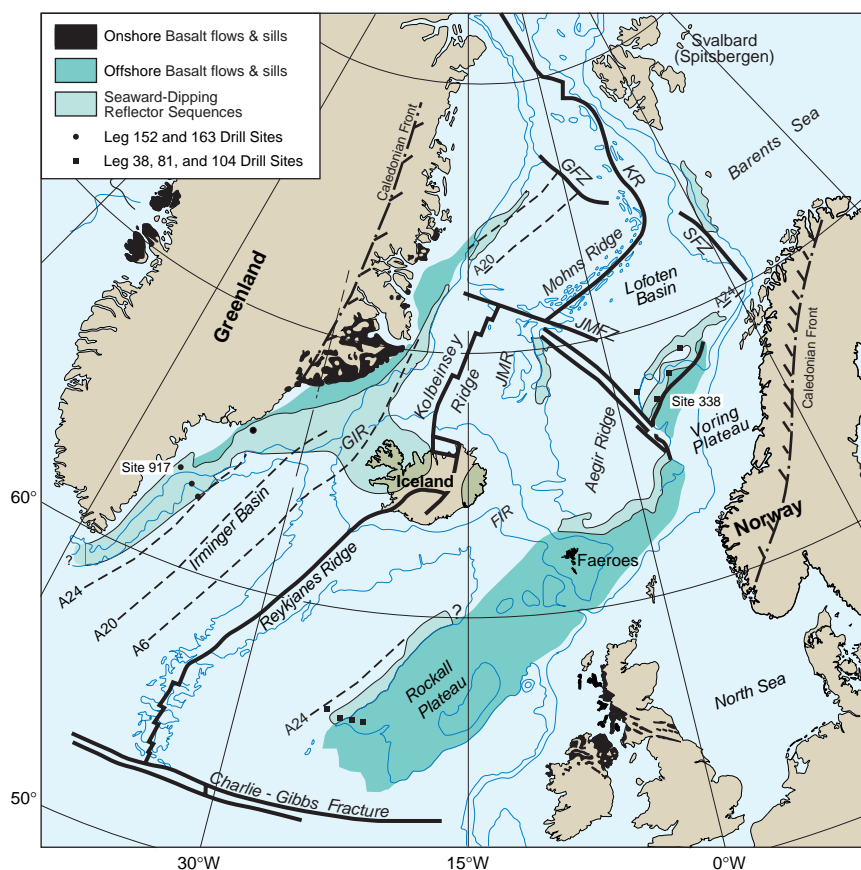


Figure 1. Location of sites from where Cr-rich spinel was analyzed. Circles show Legs 163 and 152 sites; squares show Legs 104, 81, and 38 sites (modified from Larsen, Saunders, Clift et al., 1994).

tered nature and from strong textural evidence that many have accumulated olivine. Both effects will skew whole-rock compositions to higher MgO and Mg# values. Leg 152 lavas are pervasively altered (typically >40% alteration, with loss on ignition (LOI) values to 9.5 wt%) with olivine and mesostasis completely altered and plagioclase and pyroxene usually partially altered as well. This alteration involved postemplacement hydrothermal circulation of seawater at temperatures up to 170° (Demant et al., 1988). All other cored SDRS lavas have also been affected by alteration, with complete alteration of olivine and mesostasis (Raschka and Eckhardt, 1976; Desprairies et al., 1984; Desprairies et al., 1989; Viereck et al., 1989; Parson et al., 1989; Duncan, Larsen, Allan et al., 1996). During this alteration, Mg can be exchanged for Ca on a one-to-one basis, resulting in strong depletions in rock CaO and strong enrichments in rock MgO (see Allan, 1992, and references therein). Evidence for this exchange is buttressed by the sediment pore-water geochemistry at Sites 917 and 918 from Leg 152, where dissolved Ca increased and Mg decreased as basement was approached (Larsen, Saunders, Clift, et al., 1994; Gieskes et al., 1998). In addition, accumulation of olivine during magmatic processes has also likely raised bulk-rock Mg# in the more olivine-rich Site 917 samples (Thy et al., 1998; Larsen, Saunders, Clift, et al., 1994). As a result, the compositional nature of the most primitive SDRS melts is uncertain.

In contrast to olivine and other silicate phases, Cr-rich spinel is robust in resisting alteration, and its composition is highly sensitive toward changes in host melt composition (Allan et al., 1988). In addition, the kinetics of re-equilibration of Cr-spinel with changing melt are slow in comparison with olivine, allowing zoned spinel cores and spinel inclusions to record evidence of earlier, more primitive melts than those that were erupted (Allan et al., 1988). In the SDRS lavas, Cr-spinel provides the only available tool for producing direct estimates of melt Mg#. In this paper, we use Cr-rich spinel to estimate

the Mg# of the most primitive melts in these SDRS sequences, using the algorithms of Allan (1992, 1994). These results provide first-order constraints on the extent of magmatic processes during the early opening of the North Atlantic.

## SAMPLE DESCRIPTION

Samples were chosen for analysis following initial transmitted light petrographic examination of thin sections, followed by more detailed examination of polished thin sections cut after sampling of core.

### Vøring Plateau SDRS

Despite examination of over 100 thin sections covering virtually all Leg 38 samples, Cr-rich spinel was found only in plagioclase-pyric lavas from a small portion of Leg 38 Hole 338. A general petrographic description of these rocks is given in Talwani, Udintsev, et al. (1976), but, because of sampling problems, these lavas are described in greater detail. Numerous errors exist in core photograph captions given throughout Talwani, Udintsev, et al. (1976). For the spinel-bearing cores, the published photograph of Section 38-338-43-2 is actually Section 38-338-42-3; similarly, the photograph of Section 38-338-43-3 is actually 38-338-43-2, and that of Section 38-338-43-4 is actually 38-338-43-3. The true photograph of Section 38-338-43-4 wasn't published. Cr-spinel is found within two lava flows within a mapped three-lava-flow sequence within these sections. This sequence was originally mapped as a single dike or sill by Talwani, Udintsev, et al. (1976). The top of the sequence is characterized by a nearly totally altered breccia zone; the three moderately to highly altered lava flows (here designated as Units 1, 2, and 3) are differenti-

ated by vesicle-rich zones in the manner described for the East Greenland SDRS lavas (Larsen, Duncan, Allan et al., 1995). Like the East Greenland SDRS lavas, they erupted subaerially judging from presence of the breccia zone and the lack of marginal quench. Cr-rich spinel from Leg 38 samples are found exclusively as occasional, subhedral to euhedral inclusions, from 20 to 100  $\mu\text{m}$  in size, within Unit 1 and 2 plagioclase phenocrysts. Examples of the shapes and sizes of these inclusions are given in Figure 2. Unit 1, extending from Section 38-338-42-2, 66 cm to Section 38-338-43-4, 110 cm, consists of moderately to highly plagioclase phyric basalt with a fine-grained, highly altered, holocrystalline groundmass. Plagioclase phenocrysts make up 5%–10% of the rock, are up to 3 mm in size, and commonly are found as glomerocrysts up to 1 cm in size. Isolated crystals of anhedral-subhedral clinopyroxene and euhedral olivine are greatly subordinate, making up <1% of the rock and are <1 mm in size. Olivine and the fine-grained mesostasis (30%–35%) are totally altered to greenish-brown clays. Unit 2, extending to Section 38-338-45-2, 34 cm, is less crystal rich and much less glomeroporphyritic, with 2%–3% blocky plagioclase phenocrysts (up to 5 mm) and larger amounts of anhedral-subhedral clinopyroxene and euhedral olivine (2%–3% each, up to 2 mm in size). Olivine and the fine-grained mesostasis (15%–20%) are totally altered to greenish-brown clays. Unit 3, extending to Section 38-338-45-2, 150 cm, does not contain Cr-rich spinel.

Cr-rich spinel was reported from a relatively primitive Leg 104 dike sample and as “traces of chromite as inclusions” in other unnamed samples (Viereck et al., 1989). Nevertheless, subsequent examination by the first author at the ODP East Coast Core Repository of this dike sample and of 86 other Leg 104 thin sections covering the

entire recovery found no evidence of Cr-rich spinel. A few samples from the relatively primitive chemical formation USC in Hole 642E Upper Series (with whole-rock Mg#s that average 0.68 and Cr that may exceed 300 ppm; Viereck et al., 1989) should have been able to precipitate Cr-rich spinel (e.g., Allan et al., 1988), but apparently did not. Most Leg 104 lavas are too evolved to carry Cr-rich spinel, especially those of the evolved Lower Series (Parson et al., 1989).

### Rockall Plateau SDRS

Leg 81 thin sections were unavailable for examination at the time of this study, but no reports of finding Cr-rich spinel in these samples have been made in the literature (Harrison et al., 1984; Joron et al., 1984; and Richardson et al., 1984). Moreover, few Leg 81 samples reported in these studies have Mg# higher than 0.60 and Cr higher than 300 ppm (most are well below 200 ppm Cr), with these more primitive samples being of a doleritic character and, therefore, unlikely to carry Cr-rich spinel (because of Cr partitioning into clinopyroxene and making the Cr-rich spinel unstable).

### Southeastern Greenland SDRS

Cr-rich spinel is absent from the Leg 163 lavas and from sites other than Site 917, cored during Leg 152. In contrast, petrographic analysis of the more primitive, olivine-rich lavas of Hole 917A shows them to have abundant Cr-rich spinel. Because of the extensive descriptions of these samples in Larsen, Saunders, Clift, et al. (1994), only a short, slightly modified summary is presented here. It should be noted that the Leg 152 shipboard party described unpolished thin

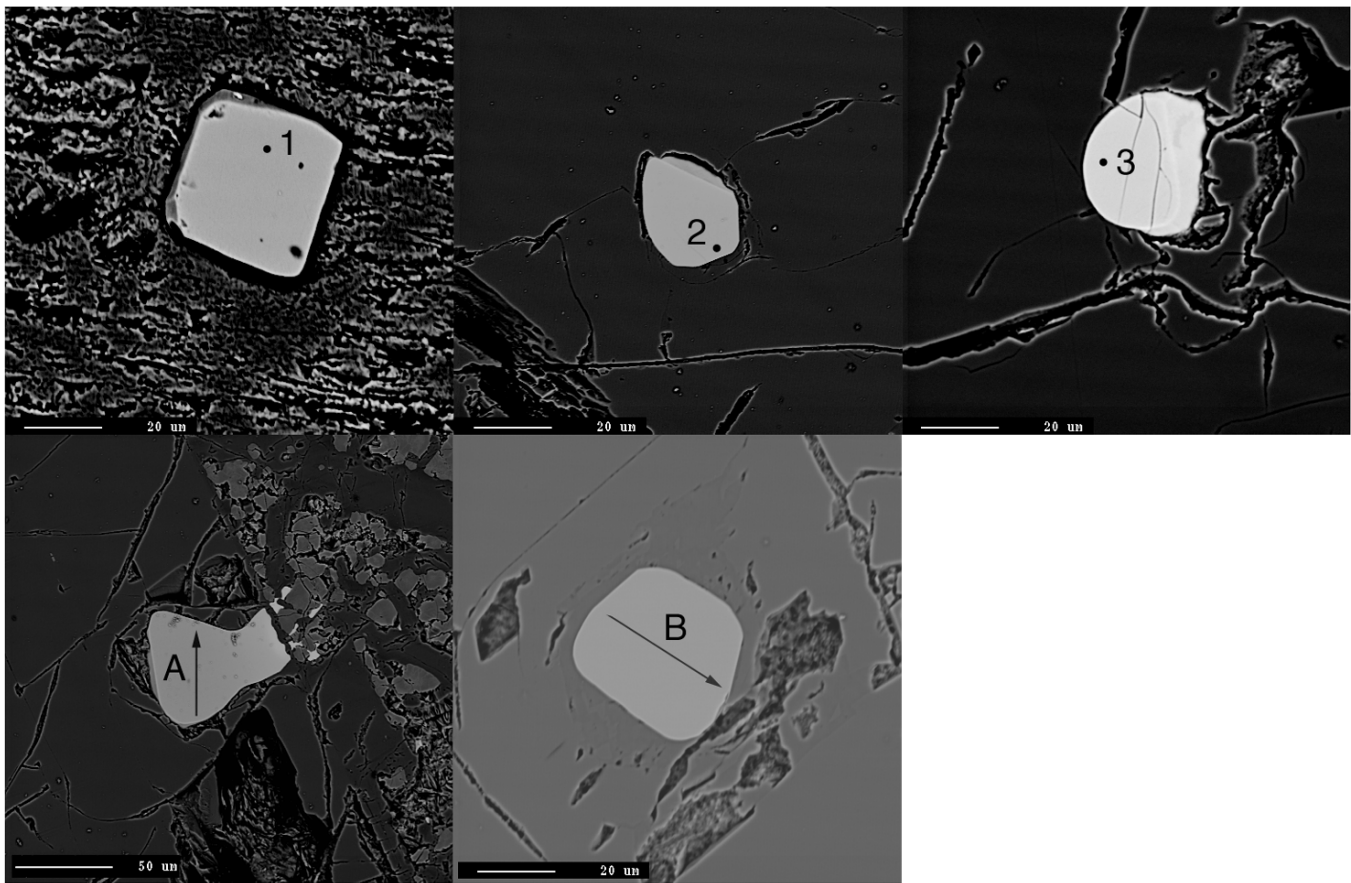


Figure 2. Backscattered electron images of examples of Cr-rich spinels from Hole 338. All represent inclusions within plagioclase. Numbers and letters represent point analyses and analytical transects given in Table 2 and Figure 7.

sections, leading to inevitable underestimates of the occurrence and abundance of Cr-rich spinel.

Larsen, Saunders, Clift, et al. (1994), amplified by Fitton et al. (1998a, 1998b), Larsen and Saunders (1988), and Saunders et al. (1998), divided the igneous recovery at Hole 917A into 92 volcanic units grouped into three subaerial igneous series. The Lower Series, comprised primarily of pahoehoe and aa basaltic lavas, and the Middle Series, comprised of evolved aa lavas and several ashflows, erupted from large, long-lived, crustally contaminated reservoirs, with shallowing of the crustal reservoirs with time. The generally more primitive Upper Series consists of thinner pahoehoe flows showing little evidence of crustal contamination and were likely erupted from smaller, more ephemeral reservoirs. Larsen, Saunders, Clift, et al. (1994) speculated that the Upper Series was derived from partial melting of more MORB-like mantle, and it represented the final phase of continental breakup of the southeast Greenland margin, with Fitton et al. (1998b) emphasizing that most of the Hole 917A suite was derived from MORB-like mantle. Other work (Fram et al., 1998) proposes that the Upper Series is actually more complex and can be broken into two groups derived from normal MORB and depleted Icelandic plume mantle, respectively.

Cr-rich spinel is found in nearly all of the aphyric olivine basalt, olivine-phyric basalt, and picrites that make up the Upper Series. Olivine phenocrysts are the differentiating feature of these lavas, with picrites defined as containing >15% olivine phenocrysts in hand sample (or >25% olivine phenocrysts in thin section) and showing evidence of olivine accumulation (Larsen, Saunders, Clift, et al. 1994). Olivine-phyric basalts were defined as containing from 1%–15% olivine phenocrysts in hand specimen (15%–22% olivine in thin section); olivine phenocrysts are uncommon but visible in hand specimen in the most commonly present aphyric olivine basalt (but contain 5%–18% olivine in thin section).

Cr-rich spinel is absent from the evolved Middle Series and from the more evolved aphyric basalts and plagioclase-dominated basalts of the Lower Series. Nevertheless, it is found abundantly in the more primitive picrites and olivine-phyric basalts of the Lower Series, and is also found in the Lower Series aphyric olivine basalts, olivine-plagioclase-phyric basalts (1%–5% olivine phenocrysts and 1%–8% plagioclase phenocrysts), and olivine-plagioclase-pyroxene basalts (>1% olivine, plagioclase, and clinopyroxene phenocrysts).

The groundmass of both Upper and Lower Series lavas may be quite coarse, with subophitic and holocrystalline, intergranular textures commonly defined by the groundmass plagioclase, clinopyroxene, and Ti-rich magnetite. They are moderately to heavily altered, with all of the olivine and fine-grained mesostasis altered to secondary clays, with plagioclase and pyroxene (including occasional orthopyroxene) usually being partially altered as well. The most olivine-rich samples—the picrites and olivine-phyric basalts—are typically the most altered.

Cr-rich spinel is most abundantly found as euhedral inclusions in olivine or as euhedral crystals embedded along the sides or edges of olivine, but loose groundmass crystals are also common. Back-scattered electron (BSE) images of representative Cr-rich spinel crystals are given in Figures 3 and 4. Cr-rich spinel is most abundant and largest in size in the most primitive samples (e.g., the picrites and olivine-phyric basalts). Groundmass Cr-rich spinels (Fig. 3) are jacketed by thick rims of chromian magnetite (ferritchromite) and Ti-rich magnetite, with the Ti-rich magnetite often exhibiting trellis exsolution of ilmenite (Sample 152-917A-11R-4, 45–50 cm, in Fig. 3). These spinels commonly show dissolution textures in conjunction with the chromian magnetite and Ti-rich magnetite jackets (Fig. 3B, C), with near-total degradation of smaller Cr-rich spinel grains (Fig. 3B). In some cases, these textures could possibly represent rapid Ti-rich magnetite growth and formation of chromian magnetite in concert with Cr-rich spinel dissolution (P. Roeder, pers. comm., 1996). Ti-rich magnetite often nearly completely replaces the previous Cr-

rich spinel, evidenced by only very small relict cores; as a result, it is difficult to avoid underestimation of Cr-rich spinel magmatic occurrence. Cr-rich spinel is best preserved in the Hole 917A lavas when it is wholly enclosed within olivine, as crystal surfaces embedded within olivine lack Ti-rich magnetite rims.

## ANALYTICAL METHODS

Sample selection for Cr-rich spinel analysis was performed in several steps. Upon review of all available Leg 38 and all Leg 152 shipboard thin sections, an initial selection of the most promising samples for Cr-rich spinel analysis was made. Every effort was made to sample as closely as possible to intervals of core that had been previously analyzed; sampling was typically done within 10–20 cm of published analyses and always within 50 cm. Splits of these samples were pulverized in a Spex Al-ceramic shatterbox barrel and analyzed by instrumental neutron activation analysis (INAA) to provide a geochemical foundation for placing the Cr-rich spinel analyses in their proper petrological context. Samples (150–200 mg in size) were irradiated for 14 hr in the Texas A&M University (TAMU) TRIGA reactor and counted for 3 hr apiece at 8 to 11 and 40 to 43 days, using facilities in the Center for Chemical Characterization, TAMU. Detailed descriptions of analytical procedures are given in Allan (1995). To ensure run-to-run consistency, a sample of the international basalt standard BHVO was run with each individual group of standards and unknowns, showing excellent overall agreement with accepted values (Table 1) (Gladney and Roelandts, 1988). INAA results for samples chosen for Cr-rich spinel analysis are given in Table 1, complemented by X-ray fluorescence (XRF) analyses by other authors for nearby samples from the same unit. INAA results for samples not chosen for Cr-rich spinel analysis are given in the Appendix.

From this set of initial samples, polished thin sections were made for transmitted and reflective light petrographic analysis. From this set, a smaller subset, covering all Cr-rich spinel-bearing rock types, was selected for major- and minor-element analysis by electron microprobe. The primary criteria for selecting samples was the presence of well-preserved Cr-rich spinels that most likely reflected compositional equilibria with melt upon eruption, rather than spinels that had obviously re-equilibrated with evolving interstitial melt during lava cooling (e.g., coarse-grained samples whose spinels uniformly had thick jackets of chromian magnetite and Ti-rich magnetite were avoided). Electron microprobe analyses were made on the TAMU Geology and Geophysics Department Cameca SX-50 microprobe, equipped with autofocus, an optically-encoded stage, and extensive Sun workstation-based image-processing capabilities. Natural (Jarosewich et al., 1980) and synthetic standards were used, as was a focused beam, sample currents of 10–30 nA, and counting times of 10–180 s. All Cr-rich spinels were initially analyzed by BSE imaging to map out compositional zoning and to avoid regions of obvious Ti-rich magnetite and chromian magnetite during further analysis. Most Cr-rich spinel grains were analyzed by automated rim-to-rim analytical traverses of individual Cr-spinel crystals for all major and minor (>0.2%) elements; very small crystals were checked for zoning by two or three analyses running from core to rim.

## ANALYTICAL RESULTS

Electron microprobe point analyses of the SDRS Cr-rich spinels are given in Table 2 and Figures 5 and 6. These analyses are keyed to the BSE images in Figures 2 and 4 either by analytical number or by transect letter label, with the analytical point in the transects given by distance in micrometers from the point of transect origin. Arrows show the direction of analysis for the analytical transects mapped in Figures 2 and 4, which are analytically shown in Figures 7 and 8. In

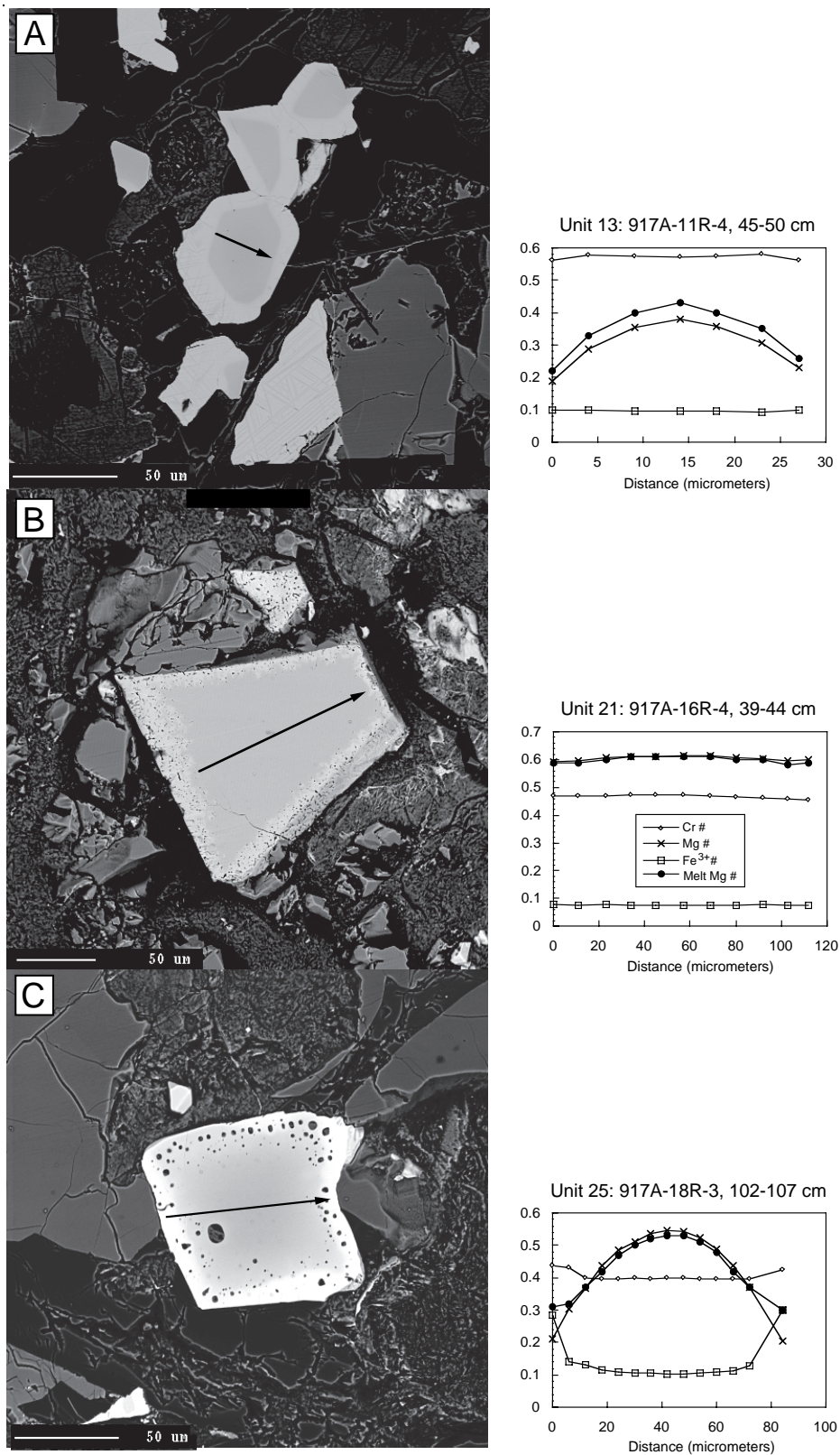


Figure 3. Examples from Hole 917A of re-equilibration in groundmass Cr-rich spinels shown by BSE images, with analytical transects also shown.  $Cr\# = Cr/(Cr + Al + Fe^{3+})$ ,  $Mg\# = Mg/(Mg + Fe^{2+})$ ,  $Fe\# = Fe^{3+}/(Cr + Al + Fe^{3+})$ , and  $Melt\ Mg\# = Melt\ Mg/(Mg + Fe^{2+})$  inferred from Cr-rich spinel compositions as explained in the text. **A.** Sample 152-917A-11R-4, 45–50 cm, shows relict Cr-rich spinel cores surrounded by Ti-rich magnetite rims exsolved to magnetite and blades of ilmenite. **B.** Sample 152-917A-16R-4, 39–44 cm, shows partially digested Cr-rich spinels with spongy margins representing Ti-rich magnetite and chromian magnetite. **C.** Sample 152-917A-18R-3, 102–107 cm, shows a Cr-rich spinel core, possibly partially digested, surrounded by magnetite and chromian magnetite.

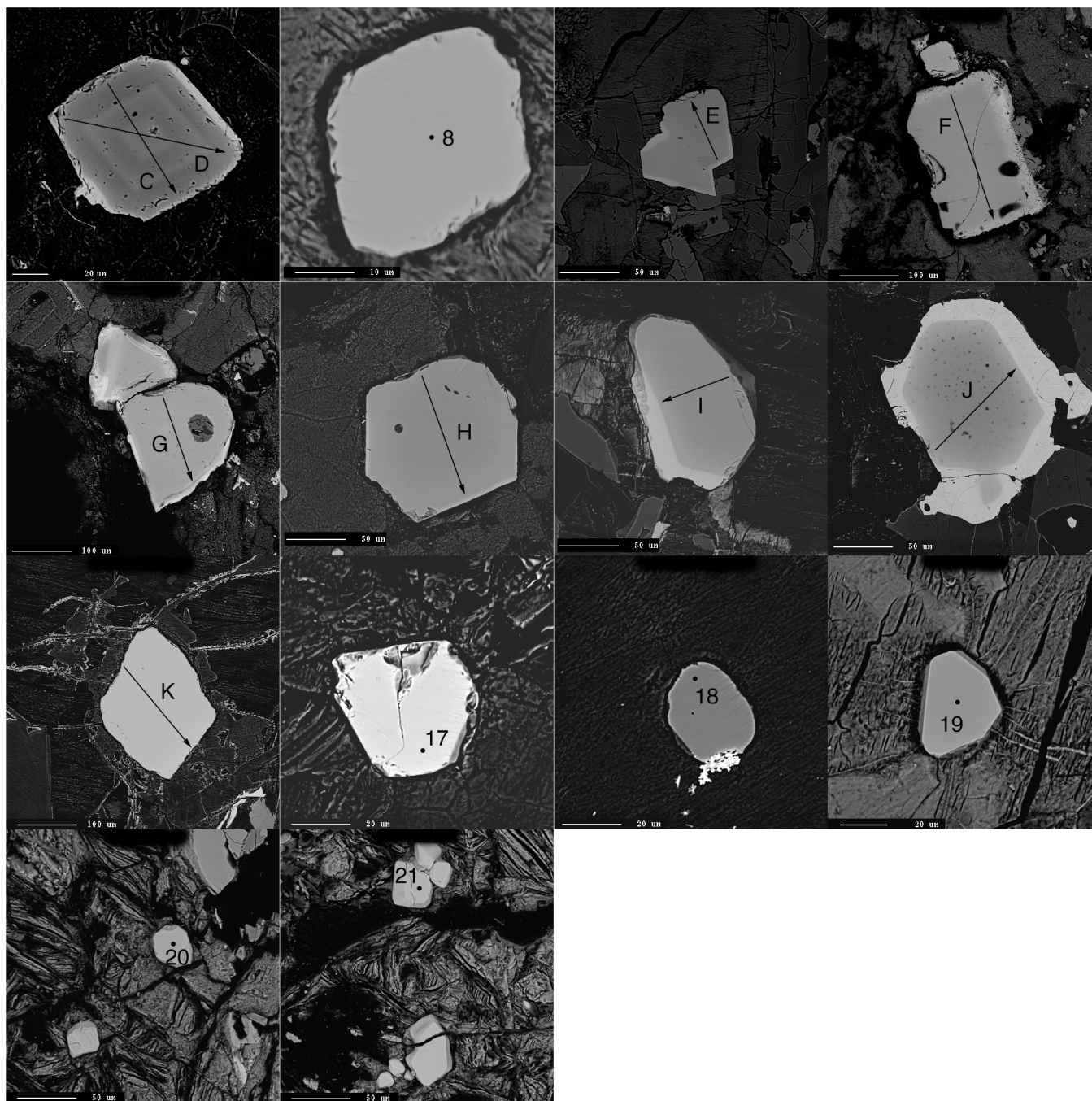


Figure 4. BSE images of examples of Cr-rich spinels from Hole 917A. All spinels given represent inclusions within or attached and partially embedded within altered olivine phenocrysts. Numbers and letters represent point analyses and analytical transects given in Table 2 and Figure 8.

general, Cr-rich spinels in this study are classified as chromium spinels or magnesiocromites, using the criteria and terminology of Sigurdsson (1977). They approximate the formula  $(\text{Mg}, \text{Fe}^{2+})(\text{Al}, \text{Cr}, \text{Fe}^{3+})_2\text{O}_4$ , and have minor  $\text{TiO}_2$  (most have 0.4%–0.8%, but rarely are as high as 2.6%),  $\text{NiO}$  (= 0.31%), and  $\text{MnO}$  (= 0.50%). Microprobe analyses of Cr-rich spinel are found in Table 3 (in ASCII format on the CD-ROM, backpocket, this volume).

Figure 5 shows all Cr-rich spinel analyses obtained in this study, plotted by mapped unit number. In examining the data, it is apparent that an enormous range in Cr-rich spinel composition exists within single units, exhibited particularly by  $\text{Mg}/(\text{Mg} + \text{Fe}^{2+})$  ( $\text{Mg}\#$ ) at a

given  $\text{Cr}/(\text{Cr} + \text{Al} + \text{Fe}^{3+})$  ( $\text{Cr}\#$ ). The origin of this variation can be understood by considering the examples given in Figure 3. In Figure 3A, a large decrease in the  $\text{Mg}\#$  is found away from the spinel core, accompanied by little change in  $\text{Cr}\#$  or  $\text{Fe}^{3+}/(\text{Cr} + \text{Al} + \text{Fe}^{3+})$  ( $\text{Fe}^{3+}\#$ ). This exchange of divalent cations without movement of the less mobile trivalent cations is common where Cr-rich spinel is rapidly re-equilibrating with a quickly evolving interstitial melt before, or more typically, after eruption, and it is equivalent to what happens under spinel metamorphic re-equilibration (Allan and Dick, 1996; Allan, 1992, 1994; Sack, 1980; Engi and Evans, 1980; Roeder et al., 1979). These exchanges may also occur during extensive alteration of the la-

Table 1. Whole-rock analyses.

Leg. hole:	38-338			152-917A										BHVO			
Core, section:	43-1	43-3	45-1	9R-1	11R-4	16R-4	18R-3	19R-4	20R-1	55R-4	64R-1	92R-4	101R-4	(Six)	S.D.	Accepted	S.D.
Interval (cm):	102-107	117-121	62-65	5-10	45-50	39-44	102-107	38-43	9-14	22-27	75-80	57-64	35-40				
Unit: Series:	1	1	2	7 Upper	13 Upper	21 Upper	25 Upper	31A Upper	31B Upper	60 Lower	68 Lower	87 Lower	92 Lower				
<b>XRF</b>																	
SiO <sub>2</sub>	47.03	48.16	46.97	47.73	44.34	46.86	46.98	46.08	48.78	48.79	48.38	50.24					
TiO <sub>2</sub>	1.01	1.10	1.18	1.27	1.12	1.69	1.86	1.47	1.55	1.41	1.09	1.16					
Al <sub>2</sub> O <sub>3</sub>	15.83	15.18	15.36	14.82	10.34	12.02	13.21	11.52	14.71	15.52	16.19	16.24					
Fe <sub>2</sub> O <sub>3</sub>	10.43	10.75	12.59	12.22	13.63	14.11	13.72	13.47	12.15	11.14	11.09	9.49					
MnO	0.12	0.23	0.21	0.19	0.21	0.23	0.22	0.18	0.17	0.16	0.14	0.2					
MgO	8.83	7.95	10.46	10.79	25.35	18.09	13.59	18.41	9.25	7.94	9.31	8.13					
CaO	10.33	11.74	10.87	10.89	4.07	7.92	8.82	7.36	12.11	12.19	10.45	12.55					
Na <sub>2</sub> O	2.27	2.20	1.76	2.05	0.7	1.42	1.74	1.28	2.06	1.91	2.33	2.24					
K <sub>2</sub> O	0.08	0.09	0.24	0.04	0.02	0.13	0.24	0.13	0.12	0.29	0.16	0.19					
P <sub>2</sub> O <sub>5</sub>	0.08	0.08	0.05	0.06	0.07	0.12	0.13	0.1	0.12	0.13	0.13	0.13					
Total	96.01	97.48	99.67	100.04	99.84	102.57	100.49	99.97	101.01	99.47	99.25	100.53					
LOI	3.88	2.83	3.08	2.1	9.51	5.51	5.12	5.01	0.12	1.61	4.08	3.32					
Mg#	0.651	0.619	0.646	0.660	0.804	0.738	0.685	0.750	0.626	0.611	0.649	0.653					
V	260	311	304	286	222	383	386	328	393	333	260	302					
Cr	323	218	359	365	998	753	518	995	309	240	416	678					
Ni	101	86	194	223	1257	626	438	866	189	107	262	252					
Cu	86	156	59	126	62	86	116	103	133	107	74	115					
Zn	72	93	74	74	76	89	88	83	73	74	77	80					
Rb			6.9	4.6	5.1	6.9	9.8	8.0	4.9	7.8	4.3	4.2					
Sr	136	128	96	116	23	100	120	92	184	228	319	360					
Y	16	24	26	26	24	27	29	26	27	26	25	26					
Zr	54	62	52	55	58	83	82	67	92	93	64	60					
Nb			1.0	1.2	2.3	3.7	4.4	3.5	7.6	8.3	2.4	3.6					
<b>INAA</b>																	
Na (%)	1.73	1.69	1.8	1.26	1.48	0.75	1.29	1.39	1.08	1.64	1.6	2.31	1.58	1.58	0.07	1.68	0.05
Fe (%)	6.31	6.96	7.85	8.56	8.51	8.1	9.2	8.95	8.78	8.5	7.45	7.35	6.94	8.60	0.15	8.55	0.15
Sc	44.0	42.5	50.1	41.1	39.0	22.6	32.5	36.7	30.2	38.5	37.5	35.7	37.2	31.2	0.4	31.8	1.3
Cr	349	352	217	412	441	1260	909	713	1310	386	291	514	804	296	9	289	22
Co	45.8	44.7	49.0	59.2	58.7	94.0	70.9	60.4	80.4	52.4	44.0	53.9	57.6	45.2	0.6	45	2
Ni	75	66	68	172	211	1130	574	415	844	192	85	171	275	114	20	121	2
Zn	88	85	105	96	89	71	85	80	85	81	75	94	97	104	13	105	5
La	3.86	3.83	4.1	1.48	1.85	2.21	4.75	4.86	3.8	6.8	8.4	9.64	6.57	15.5	0.3	15.8	1.3
Ce	8.63	8.80	9.25	4.43	6.66	10.3	14.4	14.7	16.9	16.8	18.9	22.8	17.7	37.9	0.7	39	4
Sm	2.42	2.36	2.58	2.33	2.44	2.23	3.94	4.15	3.2	3.86	3.45	3.58	3.33	6.28	0.13	6.2	0.3
Eu	0.96	0.93	1.01	0.97	0.97	0.77	1.30	1.42	1.12	1.31	1.26	1.22	1.24	2.04	0.05	2.06	0.08
Tb	0.55	0.47	0.52	0.57	0.46	0.43	0.80	0.74	0.56	0.76	0.48	0.63	0.52	0.93	0.10	0.96	0.08
Yb	1.71	1.75	2.33	2.03	1.94	1.53	2.32	2.32	2.06	2.06	1.89	1.78	1.82	1.84	0.04	2.02	0.20
Lu	0.25	0.25	0.31	0.28	0.26	0.21	0.34	0.34	0.26	0.31	0.25	0.26	0.25	0.24	0.01	0.291	0.026
Hf	1.76	1.61	1.85	1.62	1.59	1.50	2.77	2.64	2.28	2.93	2.88	1.94	1.69	4.59	0.17	4.38	0.22
Ta	0.20	0.21	0.20	ND	ND	0.05	0.19	0.15	0.15	0.40	0.48	0.14	0.17	1.17	0.09	1.23	0.13
Th	ND	0.26	ND	ND	ND	ND	0.21	0.19	0.26	0.66	0.86	0.41	ND	1.16	0.08	1.08	0.15

Notes: S.D. = standard deviation. Oxides in wt%, others in ppm. Mg# = Mg/(Mg + Fe), assuming 90% of Fe is ferrous. LOI = loss-on-ignition; ND = not detected (below detection limits). XRF Data for Leg 152 samples from Larsen, Saunders, Clift, et al. (1994). XRF Data from Leg 38 samples from Talwani, Udintsev, et al. (1976)

va, as demonstrated by Allan (1992). In the example shown in Figure 3C, the margins of the analytical transect show more profound exchange, with the sharp increase in Fe<sup>3+</sup> causing the increase in Fe<sup>3+</sup>#. Interestingly, the moderate increase in Cr# is caused by a sharp decrease in Al<sub>2</sub>O<sub>3</sub> at the margins (from 27% to 10%), likely associated with both the increase in Fe<sup>3+</sup> and the strong compositional couple between Al<sup>3+</sup> and Mg<sup>2+</sup> in the spinel structure (Sack and Ghiorso, 1991a; MgO decreases from 12% to 5%). The sharp increases in Fe<sup>3+</sup># with small declines in Mg# shown in Figure 3C are associated with similar processes of exchange and chromian magnetite formation on Cr-rich spinel margins during extended lava cooling, where interstitial melt fO<sub>2</sub> may increase and Mg# decreases substantially.

As mentioned above, Cr-rich spinel inclusions in olivine and especially plagioclase can be protected from the effects of changing melt composition and alteration, avoiding the formation of magnetite jackets and extensive re-equilibration to lower Mg#. Nevertheless, exchange with melt, especially by the divalent cations, may occur by diffusion through olivine, as was documented by Scowen et al. (1991) for Cr-rich spinels within evolving magma in the Kilauea Iki lava lake. In the Hole 917A lavas, Cr-rich spinel inclusions completely enclosed within olivine may lack magnetite jackets, but many do show, nonetheless, evidence for re-equilibration by exhibiting de-

creasing Mg# decline toward their margins. Although plagioclase is usually quite effective at "armoring" Cr-rich spinels against re-equilibration, some Hole 338 spinel inclusions also show signs of re-equilibration, perhaps aided by cracks within the plagioclase.

As the primary intention of this paper is to identify primitive melts within the SRDS system and the melt compositions existing during eruption and not to study the effects of evolving interstitial melt after eruption or Cr-rich spinel magmatic and metamorphic alteration, Figure 6 shows a cleaned data set consisting only of Cr-rich spinel analyses from unzoned crystal cores. For spinels with profiles shown in Figures 3A and 3C, the entire analytical transect was not considered, as it is not clear from the calculated Mg#s whether any relict core composition is preserved. For other spinel grains where strong zoning was observed, only the analyses of the unzoned interiors were plotted, where a significant plateau in Mg# was present. Examples of these plateaus are given in Figure 8, with the interiors of Transects E, G, and J representing marginal cases because of having a poorly developed plateau. The data from the transect shown in Figure 3B was also included in Figure 6, as the interior of the Cr-rich spinel was unzoned. Comparison of this groundmass Cr-rich spinel with Cr-rich spinel inclusions from the same sample show it to have markedly lower Mg# (see Transects F and G in Fig. 8), either reflecting a mixed

Table 2. Representative Cr-rich spinel analyses.

Leg, hole:	38-338					152-917A															
Core, section:	43-1	43-1	43-1	43-3	45-1	9R-1	9R-1	11R-4	11R-4	16R-4	16R-4	16R-4	18R-3	18R-3	19R-4	20R-1	55R-4	64R-1	92R-4	101R-4	101R-4
Sample (cm):	102-107	102-107	102-107	117-121	117-121	5-10	5-10	45-50	45-50	39-44	39-44	39-44	102-107	102-107	38-43	9-14	22-27	75-80	57-64	35-40	35-40
Description:	Inclusion core	Inclusion rim	Inclusion rim	Inclusion rim	Inclusion 2	Ol edge	Ol edge	Inclusion core	Inclusion 13	Inclusion 21	Inclusion 21	Inclusion 21	Inclusion 25	Ol edge 25	Ol edge 31A	Inclusion 31B	Inclusion rim 60	Inclusion rim 68	Inclusion 87	Inclusion core 92	Inclusion core 92
Unit:	1	1	1	1	2	7	7	13	13	21	21	21	25	25	31A	31B	60	68	87	92	92
Transect:				A	B	C	D		E	F	F	G	H	I	J	K					
Analysis number:	1	2	3	4	5	6	7	8	9	10	11	12	13	14	15	16	17	18	19	20	21
SiO <sub>2</sub>	0.08	0.02	0.05	0.09	0.06	0.11	0.10	0.05	0.05	0.05	0.06	0.06	0.04	0.03	0.07	0.08	0.06	0.16	0.07	0.11	0.06
TiO <sub>2</sub>	0.42	0.66	0.70	0.76	0.42	0.46	0.46	1.45	0.46	0.59	0.64	0.64	0.77	0.74	0.67	0.64	1.47	0.62	0.56	0.48	0.44
Al <sub>2</sub> O <sub>3</sub>	34.53	24.05	25.10	24.13	27.72	24.03	24.29	20.37	18.28	24.11	24.06	25.54	23.90	22.01	24.78	21.60	18.67	30.08	28.15	33.39	33.35
V <sub>2</sub> O <sub>3</sub>	0.16	0.23	0.19	0.20	0.17	0.10	0.13	0.58	0.09	0.13	0.13	0.16	0.15	0.15	0.17	0.12	0.27	0.17	0.18	0.17	0.15
Cr <sub>2</sub> O <sub>3</sub>	28.49	37.93	36.12	35.63	34.18	40.19	39.14	38.30	45.51	40.38	39.42	34.08	37.67	40.53	38.87	42.74	33.92	32.37	28.25	28.26	28.87
FeO	19.74	21.76	22.94	23.87	21.41	22.02	22.19	25.60	23.23	18.52	18.88	20.55	23.94	22.95	20.18	19.24	32.26	20.82	31.48	21.34	21.17
MnO	0.26	0.30	0.31	0.30	0.31	0.29	0.30	0.25	0.17	0.16	0.24	0.30	0.14	0.21	0.25	0.34	0.42	0.30	0.21	0.17	0.15
NiO	0.14	0.13	0.13	0.08	0.09	0.22	0.16	0.22	0.12	0.28	0.20	0.21	0.16	0.18	0.27	0.21	0.17	0.15	0.13	0.22	0.21
ZnO	0.09	0.09	0.07	0.07	0.02	0.05	0.09	0.08	0.03	0.05	0.03	0.04	0.05	0.07	0.06	0.09	0.11	0.03	0.15	0.04	0.06
MgO	15.98	13.94	14.07	13.48	14.45	12.95	12.97	12.25	11.86	15.63	15.53	15.59	13.15	13.02	14.56	15.00	10.72	13.98	10.33	15.59	15.61
CaO	0.36	0.10	0.12	0.10	0.07	0.03	0.02	0.00	0.01	0.01	0.01	0.02	0.00	0.02	0.01	0.02	0.07	1.00	0.03	0.03	0.04
Total	100.24	99.21	99.80	98.70	98.91	100.46	99.84	99.17	99.83	99.91	99.21	97.19	99.97	99.91	99.89	100.07	98.15	99.68	99.54	99.81	100.12
Fe <sub>2</sub> O <sub>3</sub>	7.66	8.15	9.19	9.60	8.15	6.40	6.76	9.26	6.88	7.07	7.47	9.92	8.52	7.77	6.96	7.25	14.84	6.96	11.82	8.49	8.38
FeO	12.85	14.42	14.66	15.23	14.08	16.26	16.11	17.27	17.04	12.16	12.16	11.62	16.27	15.96	13.91	12.71	18.91	14.56	20.85	13.70	13.63
Total	101.01	100.03	100.72	99.66	99.73	101.10	100.52	100.09	100.52	100.62	99.96	98.19	100.82	100.68	100.59	100.80	99.63	100.37	100.72	100.66	100.96
Cr/(Cr + Al)	0.356	0.514	0.491	0.498	0.453	0.529	0.519	0.558	0.625	0.529	0.523	0.472	0.514	0.553	0.513	0.570	0.549	0.419	0.402	0.362	0.367
Cr/(Cr + Al + Fe <sup>3+</sup> )	0.326	0.465	0.439	0.441	0.410	0.489	0.478	0.494	0.574	0.486	0.478	0.418	0.463	0.502	0.471	0.522	0.447	0.386	0.347	0.328	0.333
Mg/(Mg + Fe)	0.689	0.633	0.631	0.612	0.646	0.587	0.589	0.558	0.554	0.696	0.695	0.705	0.590	0.592	0.651	0.678	0.503	0.631	0.469	0.670	0.671
Fe <sup>3+</sup> /(Cr + Al + Fe <sup>3+</sup> )	0.084	0.095	0.106	0.113	0.093	0.074	0.079	0.114	0.083	0.081	0.086	0.116	0.100	0.092	0.080	0.084	0.186	0.079	0.138	0.094	0.092
Melt Mg/(Mg + Fe)	0.636	0.636	0.631	0.616	0.627	0.588	0.588	0.586	0.593	0.700	0.698	0.701	0.596	0.609	0.649	0.696	0.552	0.596	0.448	0.621	0.623

Note: FeO and Fe<sub>2</sub>O<sub>3</sub> recalculated after Carmichael (1967).

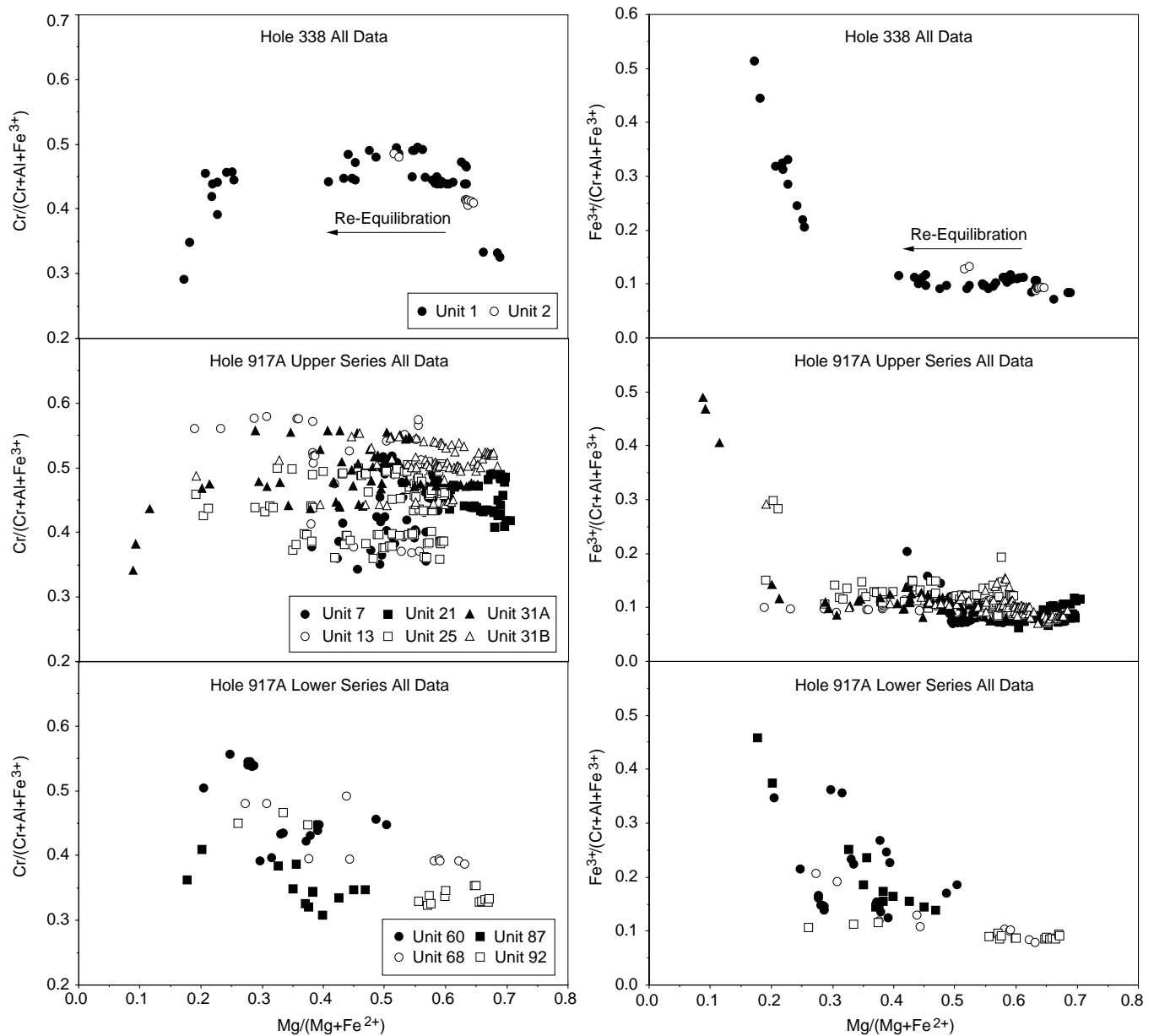


Figure 5. All Cr-rich spinel analytical data from Holes 338 and 917A, representing 483 analyses. Arrow shows primary trends resulting from Mg-Fe<sup>2+</sup> exchange during alteration or re-equilibration with evolving interstitial melt during extended lava cooling.

magma or complete re-equilibration of the spinel interior with an evolving interstitial melt after eruption. These two possibilities exist for all unzoned Cr-rich spinel cores that contain a comparatively low Mg# in samples where a broad range of spinel Mg# at a given Cr# exists.

## DISCUSSION

### Estimation of Melt Mg#

Cr-rich spinel is a proven and powerful tool for deciphering petrogenetic history of basaltic lavas and for estimating host melt Mg# (e.g., Allan et al., 1988; Sack and Ghiorso, 1991a, 1991b; Allan, 1992, 1994; Allan et al., 1996). Here we use the algorithm of Allan (1992, 1994) to calculate magmatic Mg# from the Cr-spinel composition. This algorithm has been extensively tested on a wide variety

of water-quenched alkaline and tholeiitic basalt where the quenched glass composition is known. It assumes that Cr-rich spinel behaves as an ideal reciprocal solution (Wood and Nicholls, 1978; Sack, 1982; Allan et al., 1988), that ideal mixing occurs between Mg and Fe<sup>2+</sup> in the melt, and that the pressure effect on spinel-melt equilibrium is negligible (Roeder and Reynolds, 1991). The algorithm uses a measured or assumed distribution coefficient ( $K_D$ ) for Mg-Fe<sup>2+</sup> exchange between olivine and melt to allow algebraic derivation of the spinel-melt  $K_D$  from the experimentally well-established olivine-spinel  $K_D$  (e.g., Jamieson and Roeder, 1984). As olivine is totally altered in these samples, we assume a  $K_D$  for Mg-Fe<sup>2+</sup> exchange between olivine and melt of 0.3 (Roeder and Emslie, 1970). Estimated melt compositions in equilibrium with individual Cr-rich spinel composition are given in Table 2 and in Figures 3, 7, and 8 for the analytical transects, with ranges defined from unzoned core compositions for individual samples given in Table 4. As most SDRS Cr-rich spinels

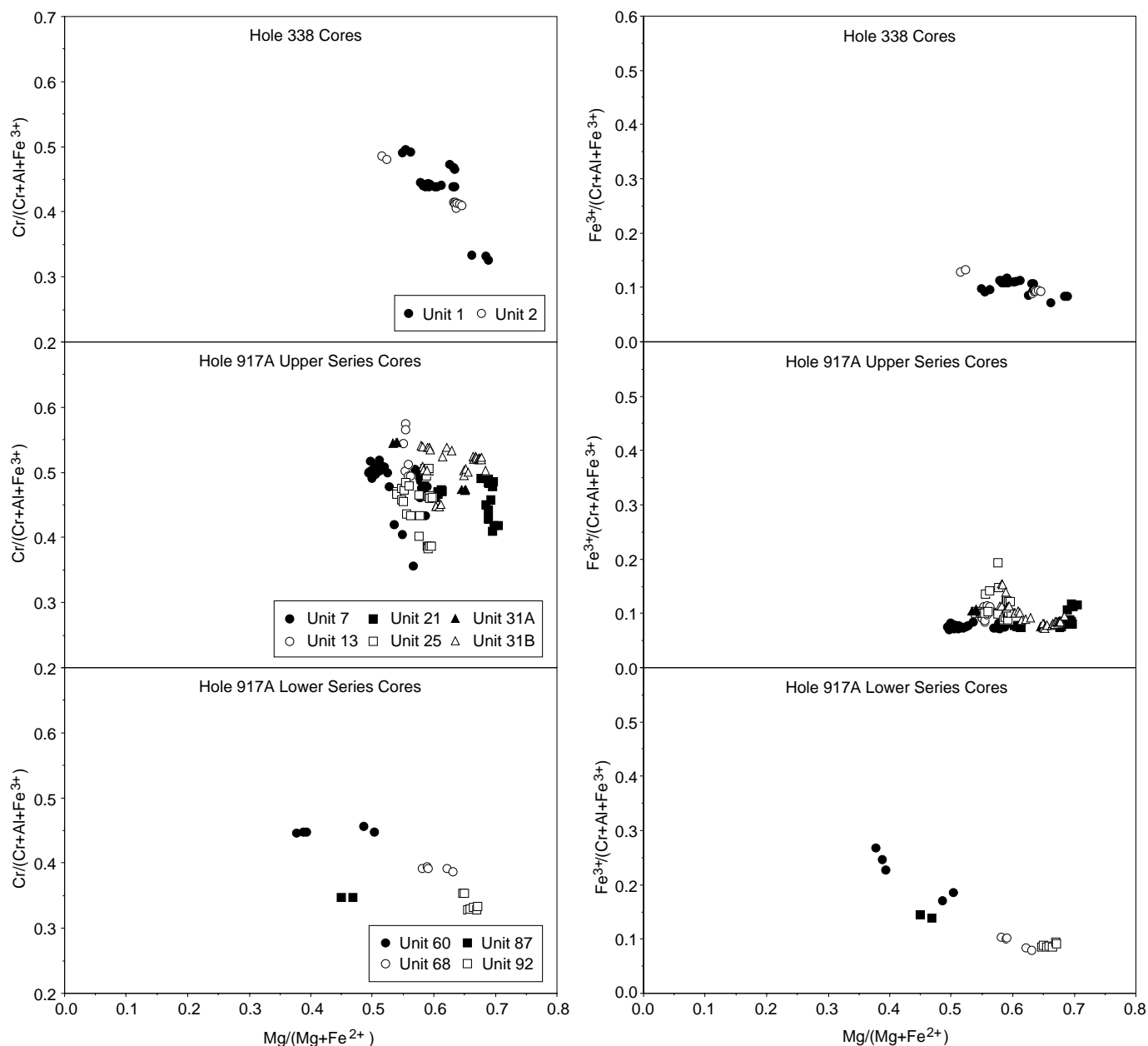


Figure 6. Compositions of unzoned Cr-rich spinel cores from Holes 338 and 917A, after removal of analyses associated with overt re-equilibration and alteration as described in text. Graphs represent 186 analyses.

have undergone at least partial re-equilibration, it is prudent to regard these inferred melt Mg# compositions as minimum estimates.

### Site 338 Cr-rich Spinel, Vøring Plateau SDRS

Cr-rich spinels within both Units 1 and 2 at Site 338 define trends of increasing Cr# with decreasing Mg#, with little variation in Fe<sup>3+</sup># (Fig. 6). These trends are commonly seen in tholeiitic basalt undergoing low-pressure olivine and plagioclase fractionation, where melt Al<sub>2</sub>O<sub>3</sub> and MgO (and Mg#) decline with increasing degree of fractionation (Allan et al., 1988). As a result, spinel Al<sub>2</sub>O<sub>3</sub> and MgO directly decline, while spinel FeO and Fe<sub>2</sub>O<sub>3</sub> increase. This effect is magnified by the reciprocal nature of the spinel solid solution, resulting from the strong coupling of Mg and Al and Fe<sup>2+</sup> and Cr. There-

fore, spinel Cr# will rise substantially as the Mg# decreases. Both units have Cr-rich spinel populations that appear to reflect spinels crystallized from a range of melt compositions, as evidenced by analyses 1, 2, and 3 in Table 2 derived from the same thin section. The simplest interpretation is that the higher Mg# Cr-rich spinels crystallized from more primitive parental magma; the original compositions of these high-Mg# spinels have been preserved by effective "armoring" afforded by the surrounding plagioclase and represent evidence of more primitive melt in the genesis of the host lava. This is consistent with the lower TiO<sub>2</sub> contents of the higher Mg# spinel (analysis 1). For both units, comparison of the analyzed whole-rock Mg# with melt Mg# inferred from the Cr-spinel compositions (Table 4) shows that these spinels crystallized from melt similar in composition to the values recorded by the whole-rock analyses and indicate

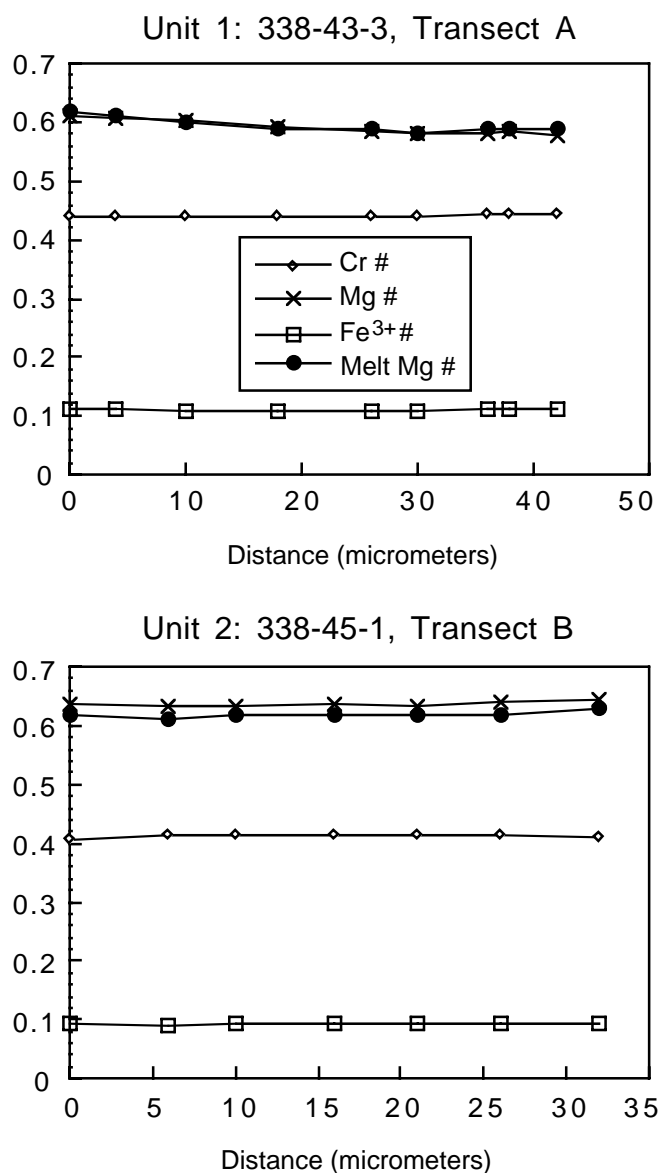


Figure 7. Analytical transects across Cr-rich spinel inclusions in plagioclase from Hole 338.  $Cr\# = Cr/(Cr + Al + Fe^{3+})$ ,  $Mg\# = Mg/(Mg + Fe^{2+})$ ,  $Fe\# = Fe^{3+}/(Cr + Al + Fe^{3+})$ , and  $Melt\ Mg\# = Melt\ Mg/(Mg + Fe^{2+})$  inferred from Cr-rich spinel compositions as explained in the text. BSE images of the crystals analyzed are given in Figure 2, with analyses from the traverses given in Table 2.

that the whole-rock compositions have been only slightly affected by alteration. The data presented here confirm that melt with Mg# as high as 0.64 erupted within the Vøring margin SDRS magmatic system.

#### Hole 917A Upper Series Cr-rich Spinel, Southeastern Greenland SDRS

Samples analyzed from this series include examples of the most primitive lavas yet cored from the North Atlantic SDRS. Cr-rich spinels from these picrites are notable for their size (to well over 200  $\mu m$ ; Figs. 4, 8) and for their generally high Mg# (Table 2; Figs. 6, 8). Slight variation in Cr# at a given Mg# and  $TiO_2$  exists within individual samples (see analyses 10–12 from Unit 21) (Table 2; Fig. 6); vari-

ations of this size are common within single-specimen spinel populations (Allan et al., 1988). The high Mg# Cr-rich spinels from the Units 21 and 31B picrites provide direct evidence that highly magnesian melts with Mg#s at least as high as 0.70 are part of the East Greenland SDRS magmatic system. Comparison with their whole-rock Mg#s (Table 4) shows that these Mg# melt estimates are lower, likely reflecting whole-rock Mg-enrichment by accumulation of olivine (as argued by Thy et al., 1998) and alteration of mesostasis.

Less magnesian-Cr-rich spinels from these units and from the Unit 25 picrite are enigmatic, as they imply that melt of significantly lower Mg# could have been present in the picrites during or after eruption. As an example, the groundmass Unit 21 Cr-rich spinel shown in Figure 3B (with a calculated Mg# of 0.62) could represent re-equilibration with evolving interstitial melt after eruption. Alternatively, the Mg# discrepancy could reflect that the actual melt in the picrite was evolved before eruption, with the high-Mg# spinel inclusions severely out of equilibrium with the host melt and representing xenocrysts. An example similar to the latter case was described by Allan (1994) for a picritic lava from Site 839 in the Lau Basin, southwest Pacific. This sample contained very large olivine and Cr-rich spinel crystals that grew from a melt with an estimated Mg# of  $>0.75$ , with both residing in quench glass with an Mg# of 0.61. These crystals were sharply zoned at their margins, with the margins in equilibrium with the glass. Apparently, magma mixing occurred immediately before eruption between highly primitive, phyrlic melt and evolved, aphyric melt. Cr-rich spinels from Unit 25 likely equilibrated with an evolved melt before or during eruption, although it is uncertain whether the interstitial melt was evolved on eruption or became evolved during cooling after eruption. It is highly unlikely that such large Cr-rich spinels in Unit 25 grew from the inferred evolved melt compositions given in Table 4; their low Mg#s likely reflect re-equilibration with evolving, interstitial melt or Mg- $Fe^{2+}$  exchange during rock alteration. The coarse-grained groundmass of this sample (Larsen, Saunders, Clift, et al., 1994) is certainly consistent with extended lava cooling and interstitial melt evolution after eruption. In any case, Units 21 and 31B Cr-rich spinels provide evidence for highly primitive melt that existed at eruption or before eruption within the East Greenland SDRS system.

Cr-rich spinels within the olivine-phyric basalt of Unit 31A also record evidence for fairly primitive compositions, although the inferred Mg# is slightly below that given by the whole-rock composition (Table 4). This difference in estimated and measured Mg# is likely caused by two factors. First, the rock is highly altered, as shown by high LOI (5.12%; Table 1). Secondly, most of the Cr-rich spinels studied in this sample were not completely protected from interstitial melt, as shown by the common presence of thick magnetite jackets (see Transect J in Fig. 4). Although an analytical plateau is shown by Transect J in Figure 8, it is not well-developed, and the core of this crystal may have been affected by a Mg- $Fe^{2+}$  exchange with evolving, interstitial melt or perhaps during rock alteration. The intergranular and subophitic nature of its coarse groundmass (Larsen, Saunders, Clift, et al., 1994) underlines the possibility of exchange with interstitial melt.

Cr-rich spinels within the aphyric olivine basalt Units 7 and 13 also provide melt Mg# estimates below that of the whole-rock analyses (Table 4), despite the presence of fairly well-developed plateaus in Transects C and D (Fig. 8). Spectacular zoning is visible in this crystal (Fig. 4); moderate decreases in Cr# (0.47–0.50 in both transects) are accompanied by slight increases in spinel Mg# expected because of crystal chemical reasons from Mg-Al and  $Fe^{2+}$ -Cr coupling (Fig. 8; see Allan et al., 1988 for similar examples). These slight increases in Mg# are superimposed on the decreasing Mg# trends (from Mg- $Fe^{2+}$  exchange with melt or during alteration) as the margins of the crystal are approached. This internal zoning, highlighted in the BSE images by the variation in Cr#, may reflect changes in spinel composition associated with magma mixing before eruption;

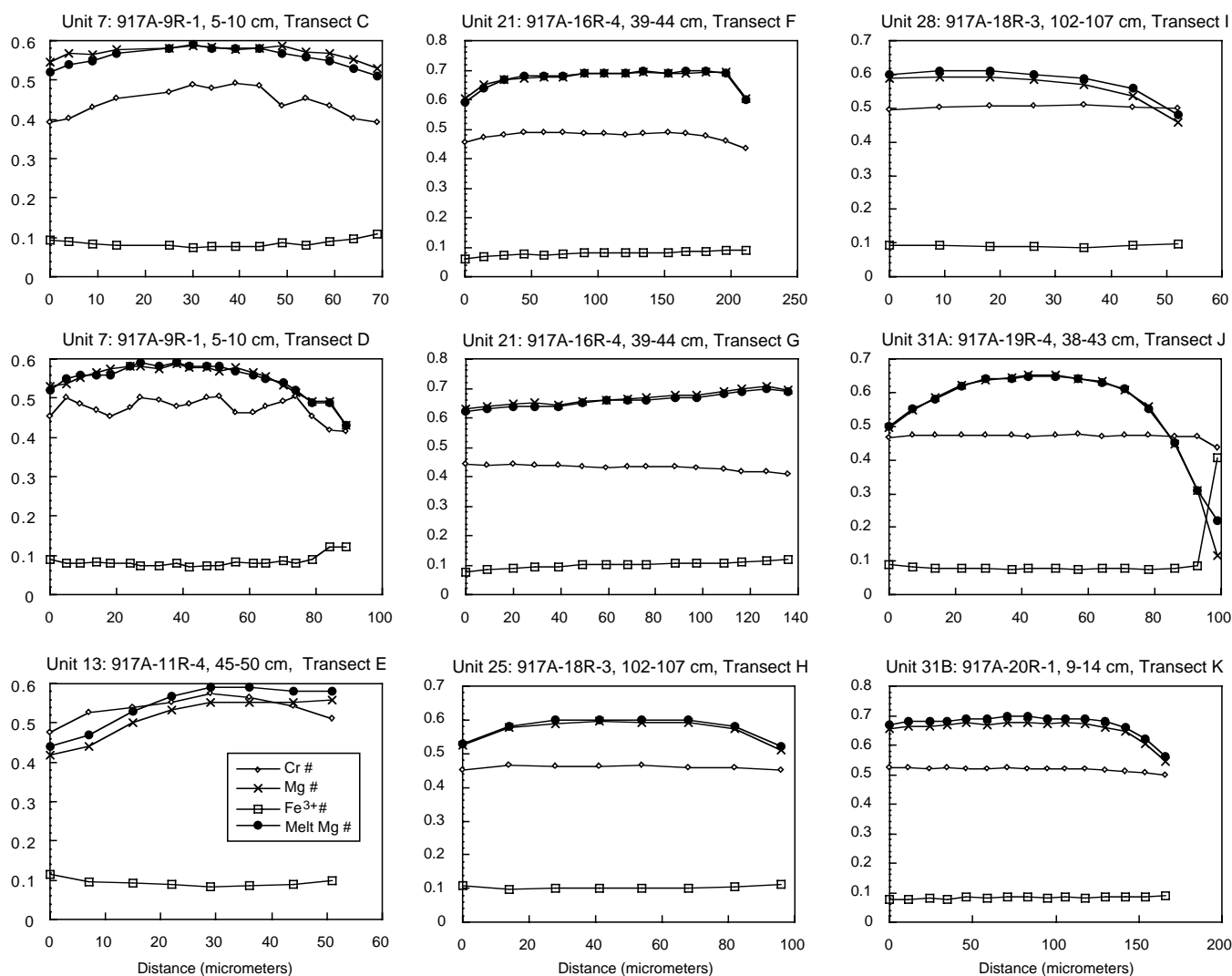


Figure 8. Analytical transects across Cr-rich spinels from Hole 917A, Upper Series. All spinels given represent inclusions within or attached and partially embedded within altered olivine phenocrysts. Cr# =  $\text{Cr}/(\text{Cr} + \text{Al} + \text{Fe}^{3+})$ , Mg# =  $\text{Mg}/(\text{Mg} + \text{Fe}^{2+})$ , Fe# =  $\text{Fe}^{3+}/(\text{Cr} + \text{Al} + \text{Fe}^{3+})$ , and Melt Mg# =  $\text{Melt Mg}/(\text{Mg} + \text{Fe}^{2+})$  inferred from Cr-rich spinel compositions as explained in the text. BSE images of the crystals analyzed are given in Figure 4, with analyses from the traverses given in Table 2.

supporting evidence is given by the broad range in the Cr# at a given Mg# of the Cr-rich spinels in this unit (Fig. 6). Evidence for magma mixing is also provided in Unit 13 by its compositionally mixed spinel population, most effectively shown by wide differences in TiO<sub>2</sub> content (see analyses 8, 9 in Table 2).

### Hole 917A Lower Series Cr-rich Spinel, Southeastern Greenland SDRS

Cr-rich spinels in the Lower Series samples are substantially smaller than those examined from the Upper Series lavas (Fig. 4), making their cores more vulnerable to the effects of post-eruptive Mg-Fe<sup>2+</sup> exchange. The more primitive Units 87 and 92 are characterized by coarse-grained groundmass (Larsen, Saunders, Clift, et al., 1994) and relatively high LOI (Table 1). For the olivine-phyric Unit 92, the relatively small disparity between the higher calculated melt Mg#s and the whole-rock Mg# (see analyses 20, 21 in Table 2) may result from a combination of olivine accumulation (the unit contains 19% altered olivine, with >8% classified as phenocrysts) (Larsen,

Saunders, Clift, et al., 1994) and alteration. Other Unit 92 Cr-rich spinels that give lower melt Mg# estimates have likely experienced some Mg loss from post-eruptive magmatic or alteration exchange. Unit 87 spinels have clearly been affected by Mg loss, leading to estimates of melt Mg# that are too low to be consistent with Cr-rich spinel growth (Table 4).

In contrast to the more primitive Lower Series samples, Units 60 and 68 are substantially fresher with finer-grained groundmass (Larsen, Saunders, Clift, et al., 1994). Estimates of melt Mg# derived from unzoned Cr-rich spinel inclusions of Unit 68 (see analysis 18 in Table 2) are in good agreement with the whole-rock analysis, supporting petrographic observations that indicate a relative lack of olivine accumulation and alteration effects.

Unzoned Cr-rich spinels from Unit 60 instead give estimates of melt Mg# substantially below that defined by the whole-rock analysis (see analysis 17 in Tables 2, 4). This sample is the only one in this study to have occasional relict cores of fresh olivine, with two very different olivine analyses from this unit reported by Demant (1998) (Fo<sub>83</sub> and Fo<sub>75</sub>). The high TiO<sub>2</sub> content (1.5%–2.6%, varying inversely

Table 4. Inferred melt compositions.

Leg, hole, core, section, interval (cm)	Unit	Description	Whole-rock Mg#	Cr-spinel cores inferred melt Mg#
38-338-43-1, 102-107	1	Plagioclase-phyric basalt		0.56-0.64
38-338-43-3, 117-121	1	Plagioclase-phyric basalt	0.651	0.58-0.62
38-338-45-1, 62-65	2	Plagioclase-olivine-clinopyroxene phyric basalt	0.619	0.55-0.63
Upper series				
152-917A-9R-1, 5-10	7	Aphyric olivine basalt	0.646	0.50-0.59
152-917A-11R-4, 45-50	13	Aphyric olivine basalt	0.660	0.58-0.59
152-917A-16R-4, 39-44	21	Picrite	0.804	0.60-0.70
152-917A-18R-3, 102-107	25	Picrite	0.738	0.55-0.61
152-917A-19R-4, 38-43	31A	Olivine-phyric basalt	0.685	0.53-0.65
152-917A-20R-1, 9-14	31B	Picrite	0.750	0.61-0.70
Lower series				
152-917A-55R-4, 22-27	60	Olivine-plagioclase-pyroxene-phyric basalt	0.626	0.46-0.55
152-917A-64R-1, 75-80	68	Olivine-plagioclase-phyric basalt	0.611	0.57-0.60
152-917A-92R-4, 57-64	87	Aphyric olivine basalt	0.649	0.43-0.45
152-917A-101R-4, 35-40	92	Olivine-phyric basalt	0.653	0.52-0.62

with spinel MgO) of these small spinel inclusions (most are below 20  $\mu\text{m}$  in size) (Fig. 4) is notable, and it implies that they grew or re-equilibrated with melt more evolved than that represented by the whole-rock composition. The highly phyric character of the sample (5%–8% olivine, 5–7% plagioclase, and 3% clinopyroxene phenocrysts in a very fine-grained matrix), and the fact that all phenocrysts are rounded and give petrographic evidence of being partially dissolved, is consistent with the variable olivine and Cr-rich spinel compositions in implying a mixed magma with a disequilibrium mineral assemblage.

### Implications for North Atlantic SDRS Composition

The results given here provide evidence that highly primitive melts erupted during the formation of the SDRS, with erupted melt Mg#s at least as high as 0.70. Another important result of this study is the conclusion that the majority of lavas erupted in the North Atlantic SDRS were too evolved to have precipitated Cr-rich spinel, especially those of the Vøring Margin. Studies of water-quenched, glassy tholeiites indicate that melt Mg# and Cr are generally >0.60 and 250 ppm, respectively, in tholeiitic melts crystallizing Cr-rich spinel (e.g., Allan et al., 1987, 1988), though this is dependent as well on  $f\text{O}_2$  (Roeder and Reynolds, 1991; Sack and Ghiorso, 1991a). Unequivocal evidence for truly primitive, near-primary melt exists only among the picrites of the Upper Series at Hole 917A, a temporally-limited part of the southeastern Greenland SDRS section. Further studies in progress may extend this evidence to cover the picrites of the Lower Series as well. The melt Mg#s inferred by the Leg 38 Cr-rich spinels indicate that these Vøring Margin melts underwent considerable fractionation after their generation in the upper mantle (for consideration of parental melts in the North Atlantic Volcanic Province see Fram and Leshner, 1993, 1997). The conclusion is that the North Atlantic SDRS are largely comprised of evolved basalts that have undergone considerable fractionation and heat loss since their generation by mantle partial melting. Recent seismic studies (Larsen et al., 1988; Dahl-Jensen et al., 1997; Korenaga et al., 1997) indicate that the Layer 3 crustal thickness underlying the SDRS basalts is abnormally thick, both in terms of total thickness and in relation to Layer 2 thickness, consistent with large amounts of fractionation of SDRS basalt parental lavas at the base of the crust or within the deep crust. This abundance of evolved SDRS basalt is both at proximal- and distal-cored SDRS sites from the inferred location of plume impact near Site 988 (Larsen, Duncan, Allan, et al., 1996), and it represents a result similar to that found by Larsen et al. (1989) for the break-up-related, East Greenland basalt of the Scoresby Sund region.

### ACKNOWLEDGMENTS

We are grateful to the staff of the ODP East and Gulf Coast Repositories for their support in collection of these samples and to the Leg 38 and 152 Scientific Parties for their useful descriptions of the cored basalt. S. Bernstein and P. Thy gave thorough and highly useful reviews, which improved the manuscript, and P. Garman did an excellent job of providing editorial suggestions. We thank USSSP for support for expenses associated with the research. Most of all, the first author is grateful for the support and friendship of his Leg 163 shipboard colleagues, many of whom put their lives at risk ensuring that Leg 163 would not end in a catastrophic loss of the ship.

### REFERENCES

- Allan, J.F., 1992. Cr-spinel as a petrogenetic indicator: deducing magma composition from spinels in highly altered basalts from the Japan Sea, Sites 794 and 797. In Tamaki, K., Suyehiro, K., Allan, J., McWilliams, M., et al., *Proc. ODP, Sci. Results*, 127/128 (Pt. 2): College Station, TX (Ocean Drilling Program), 837–847.
- , 1994. Cr-spinel in depleted basalts from the Lau backarc basin: petrogenetic history from Mg-Fe crystal-liquid exchange. In Hawkins, J., Parson, L., Allan, J., et al., *Proc. ODP, Sci. Results*, 135: College Station, TX (Ocean Drilling Program), 565–583.
- , 1995. *Data report: Trace element geochemistry of Leg 142 basalts by instrumental neutron activation analysis.* In Batiza, R., Storms, M.A., and Allan, J.F. (Eds.), *Proc. ODP, Sci. Results*, 142: College Station, TX (Ocean Drilling Program), 87–89.
- Allan, J.F., Batiza, R., and Lonsdale, P.F., 1987. Petrology and chemistry of lavas from seamounts flanking the East Pacific Rise axis, 21°N: implications concerning the mantle source composition for both seamount and adjacent EPR lavas. In Keating, B.H., Fryer, P., Batiza, R., and Boehlert, G.W. (Eds.), *Seamounts, Islands, and Atolls*. Geophys. Monogr., Am. Geophys. Union, 43:255–282.
- Allan, J.F., and Dick, H.J.B., 1996. Cr-rich spinel as a tracer for melt migration and melt-wall rock interaction in the mantle: Hess Deep, Leg 147. In Mével, C., Gillis, K.M., Allan, J.F., and Meyer, P.S. (Eds.), *Proc. ODP, Sci. Results*, 147: College Station, TX (Ocean Drilling Program), 157–172.
- Allan, J.F., Falloon, T., Pedersen, R.B., Shankar Lakkapragada, B., Natland, J.H., and Malpas, J., 1996. Petrology of selected Leg 147 basaltic lavas and dikes. In Mével, C., Gillis, K.M., Allan, J.F., and Meyer, P.S. (Eds.), *Proc. ODP, Sci. Results*, 147: College Station, TX (Ocean Drilling Program), 173–186.
- Allan, J.F., Sack, R.O., and Batiza, R., 1988. Cr-rich spinels as petrogenetic indicators: MORB-type lavas from the Lamont seamount chain, eastern Pacific. *Am. Mineral.*, 73:741–753.
- Basaltic Volcanism Study Project (BSVP), 1981. *Basaltic Volcanism on the Terrestrial Planets*: New York (Pergamon Press).

- Campbell, I.H., and Griffiths, R.W., 1990. Implications of mantle plume structure for the evolution of flood basalts. *Earth Planet. Sci. Lett.*, 99:79–93.
- Carmichael, I.S.E., 1967. The iron-titanium oxides of salic volcanic rocks and their associated ferromagnesian silicates. *Contrib. Mineral. Petrol.*, 14:36–64.
- Dahl-Jensen, T., Holbrook, W.S., Hopper, J.R., Korenaga, J., Larsen, H.C., Detrick, R.S., and Kent, G.M., 1997. Structure of upper crust at the SE Greenland volcanic rifted margin out to Chron 21 times. *Eos*, 78:668–669.
- Demant, A., 1998. Mineral chemistry of volcanic sequences from Hole 917A, southeast Greenland Margin. In Saunders, A.D., Larsen, H.C., and Wise, S.W., Jr. (Eds.), *Proc. ODP, Sci. Results*, 152: College Station, TX (Ocean Drilling Program), 403–416.
- Demant, A., Münch, P., Romeuf, N., and Morata, D., 1998. Distribution and chemistry of secondary minerals (zeolites and clay minerals) from Hole 917A, southeast Greenland Margin. In Saunders, A.D., Larsen, H.C., and Wise, S.W., Jr. (Eds.), *Proc. ODP, Sci. Results*, 152: College Station, TX (Ocean Drilling Program), 417–424.
- Desprairies, A., Bonnot-Courtois, C., Jehanno, C., Vernhet, S., and Joron, J.L., 1984. Mineralogy and geochemistry of alteration products in Leg 81 basalts. In Roberts, D.G., Schnitker, D., et al., *Init. Repts. DSDP*, 81: Washington (U.S. Govt. Printing Office), 733–742.
- Desprairies, A., Tremblay, P., and Laloy, C., 1989. Secondary mineral assemblages in a volcanic sequence drilled during ODP Leg 104 in the Norwegian Sea. In Eldholm, O., Thiede, J., Taylor, E., et al., *Proc. ODP, Sci. Results*, 104: College Station, TX (Ocean Drilling Program), 397–409.
- Duncan, R.A., Larsen, H.C., Allan, J.F., et al., 1996. *Proc. ODP, Init. Repts.*, 163: College Station, TX (Ocean Drilling Program).
- Eldholm, O., Thiede, J., Taylor, E., et al., 1987. *Proc. ODP, Init. Repts.*, 104: College Station, TX (Ocean Drilling Program).
- Engi, M., and Evans, B.W., 1980. A re-evaluation of the olivine-spinel Geothermometer: discussion. *Contrib. Mineral. Petrol.*, 73:201–203.
- Fitton, J.G., Hardarson, B.S., Ellam, R.M., Rogers, G., 1998a. Sr-, Nd-, and Pb-isotopic composition of volcanic rocks from the southeast Greenland Margin at 63°N: temporal variation in crustal contamination during continental breakup. In Saunders, A.D., Larsen, H.C., and Wise, S.W., Jr. (Eds.), *Proc. ODP, Sci. Results*, 152: College Station, TX (Ocean Drilling Program), 351–357.
- Fitton, J.G., Saunders, A.D., Larsen, L.M., Hardarson, B.S., and Norry, M.J., 1998b. Volcanic rocks from the southeast Greenland Margin at 63°N: composition, petrogenesis, and mantle sources. In Saunders, A.D., Larsen, H.C., and Wise, S.W., Jr. (Eds.), *Proc. ODP, Sci. Results*, 152: College Station, TX (Ocean Drilling Program), 331–350.
- Fram, M.S., and Leshner, C.E., 1993. Geochemical constraints on mantle melting during creation of the North Atlantic basin. *Nature*, 363:712–715.
- , 1997. Generation and polybaric differentiation of East Greenland early Tertiary flood basalts. *J. Petrol.*, 38:231–275.
- Fram, M.S., Leshner, C.E., and Volpe, A.M., 1998. Mantle melting systematics: transition from continental to oceanic volcanism on the southeast Greenland Margin. In Saunders, A.D., Larsen, H.C., and Wise, S.W., Jr. (Eds.), *Proc. ODP, Sci. Results*, 152: College Station, TX (Ocean Drilling Program), 373–386.
- Gieskes, J.M., Schrag, D., Chan, L.-H., Zhang, L., and Murray, R.W., 1998. Geochemistry of interstitial waters. In Saunders, A.D., Larsen, H.C., and Wise, S.W., Jr. (Eds.), *Proc. ODP, Sci. Results*, 152: College Station, TX (Ocean Drilling Program), 293–305.
- Gladney, E.S., and Roelandts, I., 1988. 1987 compilation of elemental concentration data from USGS BHOV-1, MAG-1, QLO-1, RGM-1, SCo-1, SDC-1, SGR-1 and STM-1. *Geostand. Newsl.*, 12:253–262.
- Harrison, R.K., Merriman, R.J., Evans, J., Hutchison, D., Davis, A.E., Holmes, K.A., Joseph, P., Judge, V.A., and Wheatley, C.W., 1984. Petrology, mineralogy, and chemistry of basaltic rocks: Leg 81. In Roberts, D.G., Schnitker, D., et al., *Init. Repts. DSDP*, 81: Washington (U.S. Govt. Printing Office), 743–774.
- Jamieson, H.E., and Roeder, P.L., 1984. The distribution of Mg and Fe<sup>2+</sup> between olivine and spinel at 1300°C. *Am. Mineral.*, 69:283–291.
- Jarosewich, E., Nelen, J.A., and Norberg, J.A., 1980. Reference samples for electron microprobe analysis. *Geostand. Newsl.*, 4:43–47.
- Joron, J.L., Bougault, H., Maury, R.C., Bohn, M., and Desprairies, A., 1984. Strongly depleted tholeiites from the Rockall Plateau margin, North Atlantic: geochemistry and mineralogy. In Roberts, D.G., Schnitker, D., et al., *Init. Repts. DSDP*, 81: Washington (U.S. Govt. Printing Office), 783–794.
- Kinzler, R.J., and Grove, T.L., 1992. Primary magmas of mid-ocean ridge basalts, 2. Applications. *J. Geophys. Res.*, 97:6907–6926.
- Klein, E.M., and Langmuir, C.H., 1987. Global correlations of ocean ridge basalt chemistry with axial depth and crustal thickness. *J. Geophys. Res.*, 92:8089–8115.
- Korenaga, J., Holbrook, W.S., Kent, G.M., Kelemen, P.B., Detrick, R.S., Dahl-Jensen, T., Hopper, J.R., and Larsen, H.C., 1997. Deep crustal structure of hotspot-influenced rifted margin: Southeast Greenland margin. *Eos*, 78:668.
- Larsen, H.C., Dahl-Jensen, T., and Hopper, J.R., 1998. Crustal structure along the Leg 152 drilling transect. In Saunders, A.D., Larsen, H.C., and Wise, S.W., Jr. (Eds.), *Proc. ODP, Sci. Results*, 152: College Station, TX (Ocean Drilling Program), 463–475.
- Larsen, H.C., and Saunders, A.D., 1998. Tectonism and volcanism at the southeast Greenland rifted margin: a record of plume impact and later continental rupture. In Saunders, A.D., Larsen, H.C., and Wise, S.W., Jr. (Eds.), *Proc. ODP, Sci. Results*, 152: College Station, TX (Ocean Drilling Program), 503–533.
- Larsen, H.C., Saunders, A.D., Clift, P.D., et al., 1994. *Proc. ODP, Init. Repts.*, 152: College Station, TX (Ocean Drilling Program).
- Larsen, L.M., Fitton, J.G., and Fram, M.S., 1998. Volcanic rocks of the southeast Greenland Margin in comparison with other parts of the North Atlantic tertiary igneous province. In Saunders, A.D., Larsen, H.C., and Wise, S.W., Jr. (Eds.), *Proc. ODP, Sci. Results*, 152: College Station, TX (Ocean Drilling Program), 315–330.
- Larsen, L.M., Watt, W.S., and Watt, M., 1989. Geology and petrology of the Lower Tertiary plateau basalts of the Scoresby Sund region, East Greenland. *Bull.—Groenl. Geol. Unders.*, 157:1–164.
- McKenzie, D., and Bickle, M.J., 1988. The volume and composition of melt generated by extension of the lithosphere. *J. Petrol.*, 29:625–679.
- Niu, Y., and Batiza, R., 1991. An empirical method for calculating melt compositions produced beneath mid-ocean ridges: application for axis and off-axis (seamounts) melting. *J. Geophys. Res.*, 96:21753–21777.
- Parson, L., Viereck, L., Love, D., Gibson, I., Morton, A., and Hertogen, J., 1989. The petrology of the lower series volcanics, ODP Site 642. In Eldholm, O., Thiede, J., Taylor, E., et al., *Proc. ODP, Sci. Results*, 104: College Station, TX (Ocean Drilling Program), 419–428.
- Raschka, H., and Eckhardt, F.-J., 1976. Geochemistry of basalt from the Norwegian-Greenland Sea, Leg 38, DSDP. In Talwani, M., Udintsev, G., et al., *Init. Repts. DSDP*, 38: Washington (U.S. Govt. Printing Office), 719–730.
- Ribe, N.M., Christensen, U.R., and Theiβing, J., 1995. The dynamics of plume-ridge interaction, 1: Ridge-centered plumes. *Earth Planet. Sci. Lett.*, 134:155–168.
- Richards, M.A., Duncan, R.A., and Courtillot, V.E., 1989. Flood basalts and hot-spot tracks: plume heads and tails. *Science*, 246:103–107.
- Richardson, C., Oakley, P.J., and Cann, J.R., 1984. Trace and major element chemistry of basalts from Leg 81. In Roberts, D.G., and Schnitker, D., et al., *Init. Repts. DSDP*, 81: Washington (U.S. Govt. Printing Office), 795–806.
- Roberts, D.G., Schnitker, D., et al., 1984. *Init. Repts. DSDP*, 81: Washington (U.S. Govt. Printing Office).
- Roeder, P.L., Campbell, I.H., and Jamieson, H.E., 1979. A re-evaluation of the olivine-spinel geothermometer. *Contrib. Mineral. Petrol.*, 68:325–334.
- Roeder, P.L., and Emslie, R.F., 1970. Olivine-liquid equilibrium. *Contrib. Mineral. Petrol.*, 29:275–289.
- Roeder, P.L., and Reynolds, I., 1991. Crystallization of chromite and chromium solubility in basaltic liquid. *J. Petrol.*, 32:909–934.
- Sack, R.O., 1980. Adirondack mafic granulites and a model lower crust: summary. *Geol. Soc. Am. Bull.*, 91 (Pt. 1):89–93.
- , 1982. Spinels as petrogenetic indicators: activity-composition relations at low pressures. *Contrib. Mineral. Petrol.*, 79:169–186.
- Sack, R.O., and Ghiorso, M.S., 1991a. Chromian spinels as petrogenetic indicators: thermodynamics and petrological applications. *Am. Mineral.*, 76:827–847.
- Sack, R.O., and Ghiorso, M.S., 1991b. An internally consistent model for the thermodynamic properties of Fe-Mg-titanomagnetite-aluminate spinels. *Contrib. Mineral. Petrol.*, 106:474–505.
- Saunders, A.D., Larsen, H.C., and Fitton, J.G., 1998. Magmatic development of the southeast Greenland Margin and evolution of the Iceland Plume: geochemical constraints from Leg 152. In Saunders, A.D., Larsen, H.C.,

- and Wise, S.W., Jr. (Eds.), *Proc. ODP, Sci. Results*, 152: College Station, TX (Ocean Drilling Program), 479–501.
- Schilling, J.-G., 1991. Fluxes and excess temperatures of mantle plumes inferred from their interaction with migrating mid-ocean ridges. *Nature*, 352:397–403.
- Scowen, P.A., Roeder, P.L., and Helz, R., 1991. Reequilibration of chromite within Kilauea Iki lava lake, Hawaii. *Contrib. Mineral. Petrol.*, 107:8–20.
- Sigurdsson, H., 1977. Spinel in Leg 37 basalts and peridotites: phase chemistry and zoning. In Aumento, F., Melson, W.G., et al., *Init. Repts. DSDP*, 37: Washington (U.S. Govt. Printing Office), 883–891.
- Sinton, C.W., and Duncan, R.A., 1998.  $^{40}\text{Ar}$ - $^{39}\text{Ar}$  ages of lavas from the southeast Greenland Margin, ODP Leg 152, and the Rockall Plateau, DSDP Leg 81. In Saunders, A.D., Larsen, H.C., and Wise, S.W., Jr. (Eds.), *Proc. ODP, Sci. Results*, 152: College Station, TX (Ocean Drilling Program), 387–402.
- Takahashi, E., and Kushiro, I., 1983. Melting of a dry peridotite at high pressures and temperatures and basalt magma genesis. *Am. Mineral.*, 68:859–879.
- Talwani, M., Udintsev, G., et al., 1976. *Init. Repts. DSDP*, 38: Washington (U.S. Govt. Printing Office).
- Thy, P., Leshner, C.E., and Fram, M.S., 1998. Low pressure experimental constraints on the evolution of basaltic lavas from Site 917, southeast Greenland continental margin. In Saunders, A.D., Larsen, H.C., and Wise, S.W., Jr. (Eds.), *Proc. ODP, Sci. Results*, 152: College Station, TX (Ocean Drilling Program), 359–372.
- Viereck, L.G., Hertogen, J., Parson, L.M., Morton, A.C., Love, D., and Gibson, I.L., 1989. Chemical stratigraphy and petrology of the Vøring Plateau tholeiitic lavas and interlayered volcanoclastic sediments at ODP Hole 642E. In Eldholm, O., Thiede, J., Taylor, E., et al., *Proc. ODP, Sci. Results*, 104: College Station, TX (Ocean Drilling Program), 367–396.
- White, R.S., Bown, J.W., and Smallwood, J.R., 1995. The temperature of the Iceland plume and origin of outward-propagating V-shaped ridges. *J. Geol. Soc. London*, 152:1039–1045.
- White, R.S., and McKenzie, D., 1989. Magmatism at rift zones: the generation of volcanic continental margins and flood basalts. *J. Geophys. Res.*, 94:7685–7729.
- Wood, B.J., and Nicholls, J., 1978. The thermodynamic properties of reciprocal solid solutions. *Contrib. Mineral. Petrol.*, 66:389–400.

**Date of initial receipt: 5 January 1998**

**Date of acceptance: 19 May 1998**

**Ms 163SR-121**

## APPENDIX

## Additional neutron activation analyses.

Leg, hole:	38- 338	38- 338	38- 338	38- 338	163- 988A	163- 989A	152- 917A	163- 990A														
Core, section:	43-2	44-2	45-2	45-2	3R2	2R3	8R-2	9R-3	10R-1	12R-2	13R-1	15R-2	17R-4	18R-6	21R-3	57R-3	79R-2	90R-5	91R-2	94R-4	96R-1	11R1
Interval: (cm)	20-24	119-121	6-11	131-136	0-13	68-81	26-31	40-45	70-75	135-140	67-72	51-56	57-63	102-107	90-95	87-92	59-64	39-44	24-29	73-78	79-85	85-98
Unit: Series:	1	2	2	3	1	1	6 Upper	8 Upper	9 Upper	15 Upper	16 Upper	19 Upper	24 Upper	27 Upper	33 Upper	61B Lower	78 Lower	86 Lower	87 Lower	87 Lower	88 Lower	2
Na (%)	1.75	1.6	1.65	1.56	1.86	1.51	1.38	1.52	1.63	1.46	1.36	1.54	1.71	1.49	1.57	0.8	1.57	1.58	1.67	1.76	1.28	1.58
Fe (%)	7.69	7.71	7.5	7.94	10.2	9.57	7.93	8.56	8.57	8.58	7.42	8.77	8.75	9.06	8.94	8.16	6.87	7.72	7.36	7.84	8.44	8.35
Sc	39.9	47.0	47.0	46.8	40.9	49.1	30.5	39.8	38.7	40.0	39.0	44.0	42.7	36.8	42.0	24.3	31.3	40.4	38.3	34.6	37.7	44.3
Cr	329	202	202	198	142	53	760	464	405	647	885	358	309	635	320	973	635	460	315	467	728	138
Co	47.5	50.1	46.0	48.3	48.5	51.8	66.0	61.6	56.5	63.6	60.7	54.4	53.5	59.7	51.9	85.8	52.8	52.6	48.8	53.7	58.0	46.2
Ni	78	56	59	69	83.5	61.2	409	240	164	294	377	135	141	372	123	465	172	99	73	161	194	61.3
Zn	92	99	102	93	134	97.8	78	68	68	85	61	84	87	86	75	85	70	87	81	91	78	86.7
La	3.59	3.8	3.96	3.94	14.5	2.41	2.73	1.35	1.93	1.13	3.66	2.98	3.06	5.31	3.32	4.15	8.06	6.27	8.04	9.97	4.71	3.98
Ce	9.47	10.8	9.63	9.36	36.3	6.33	7.04	4.65	6.87	3.62	11.5	9.63	9.05	16.1	11.2	10.8	17.7	17.2	19.9	23.9	12.0	9.41
Sm	2.22	2.33	2.49	2.52	5.71	2.3	2.35	2.28	2.67	2.18	2.68	3.29	3.35	4.49	3.27	1.98	2.56	3.25	3.61	3.66	3.58	2.25
Eu	0.86	0.92	0.97	1.00	1.96	0.87	0.92	1.01	1.10	0.97	1.05	1.31	1.19	1.53	1.22	0.75	0.89	1.17	1.27	1.31	1.31	0.86
Tb	0.55	0.48	0.58	0.62	1.13	0.84	0.51	0.54	0.53	0.59	0.44	0.70	0.89	1.05	0.81	0.29	0.55	0.70	0.70	0.65	0.70	0.68
Yb	1.63	1.94	2.06	2.01	2.96	2.98	1.89	1.94	2.12	2.27	2.09	2.14	2.12	2.67	1.98	1.05	1.53	2.04	2.00	1.91	2.34	2.44
Lu	0.23	0.29	0.29	0.30	0.38	0.40	0.24	0.26	0.27	0.30	0.30	0.28	0.29	0.35	0.27	0.14	0.19	0.27	0.26	0.25	0.27	0.33
Hf	1.46	1.49	1.70	1.96	4.49	1.72	1.53	1.50	1.81	1.40	1.79	2.12	2.20	3.31	2.41	1.18	1.34	1.70	2.02	1.93	2.55	1.49
Ta	0.23	0.21	0.20	0.20	1.06	0.12	ND	ND	ND	ND	ND	ND	0.08	0.22	0.09	0.17	0.07	0.07	ND	0.15	0.12	0.09
Th	ND	0.32	ND	ND	1.16	ND	ND	ND	ND	ND	0.32	ND	ND	ND	ND	0.22	ND	ND	ND	0.21	ND	ND

Note: ND = not detected (below detection limits).